Inverse Problems in Science and Engineering, 2016
Vol. 24, No. 2, 284–316, http://dx.doi.org/10.1080/17415977.2015.1018828

Recovery of parameters of cancellous bone by acoustic interrogation

Robert P. Gilbert, Philippe Guyenne* and Michael Shoushani

Department of Mathematical Sciences, University of Delaware, Newark, DE, USA

(*Received 30 January 2014; final version received 9 June 2014*)

The parameter recovery problem for cancellous bone by acoustic interrogation is investigated numerically. Biot's equations coupled with boundary integral equations are used to model ultrasound propagation through a bone sample immersed in a water tank. The mathematical formulation for two-dimensional orthotropic bone is presented, but numerical results are only discussed in the isotropic case. The inversion procedure consists in minimizing some error on the pressure at measurement points located outside the bone sample. For this purpose, two different minimization algorithms are considered. A number of numerical tests are performed for a range of frequencies, which demonstrate the model's ability to recover some bone parameters with satisfactory accuracy.

Keywords: Biot model; boundary integral equation; cancellous bone; minimization procedure; ultrasound

AMS Subject Classifications: 31A25; 35R30; 49N45; 74A65; 74G75; 76Q05

1. Introduction

Since 70% of the variance of bone strength is accounted for by bone density, quantitative ultrasound techniques could provide an important new diagnostic tool.[1–26] Moreover, in contrast to X-ray densitometry, ultrasound which also measures bone density does not ionize the tissue, and its implementation is relatively inexpensive. Since the loss of bone density and the destruction of bone microstructure is most evident in osteoporotic cancellous bone, which consists of trabeculae and marrow, it is natural to consider the possibility of developing accurate ultrasound models for the insonification of cancellous bone. It would be of enormous clinical advantages if accurate methods could be developed using ultrasound interrogation to diagnose osteoporosis and bone fractures.

Cancellous bone is a two-component material consisting of a calcified bone matrix with interstitial fatty marrow. Hence, mathematical models such as Biot's model for poroplastic media are applicable.[18,27–32] One particular ultrasonic technique for assessing bone mineral density is by measuring the calcaneal broadband ultrasonic attenuation (BUA) and speed of sound, which are highly correlated with calcaneal bone mineral density.[25,33] This method uses the travel time of sound between two transducers with a bone sample between them and the travel time in the absence of the specimen to determine the compressional wave velocity in the bone.

*Corresponding author. Email: guyenne@math.udel.edu

Another experiment involves measuring the spectra of the phase velocity $c(\omega)$ and of the attenuation rate $\alpha(\omega)$, where ω is the frequency of the sound wave. Many investigations reported that the attenuation is linear from 200 to 600 kHz and also from 600 kHz to 1 MHz,[16,17,19] i.e. $\alpha(\omega)$ is assumed to be a linear function as $\alpha(\omega) = \text{BUA}\,\omega + K$ with K being a constant. The BUA coefficient is the gradient in dB/MHz evaluated by linear regression and is thought relevant to the evaluation of osteoporosis.[7] Hoffmeister et al. [34] found that, in the range 0.5–1 MHz, BUA exhibits a significant correlation with the anterior–posterior and medial–lateral directions but not in the superior–inferior orientation. A break point in the slopes was observed at about 1 MHz, whereas other researchers observed one at about 400 kHz. Others observed measurable nonlinear attenuation at frequencies below 400 kHz for unfatted bone from human cadavers.[23] Langton et al. [17] found that the BUA value of the ultrasonic spectrum measured on the calcaneus is significantly lower in older women with osteoporotic fracture compared to younger women without these fractures. However, Chaffai et al. [4] found that attenuation varies in terms of frequency roughly as $\omega^{1.1\pm0.3}$.

Hodgskinson et al. [35] found that density is a good predictor of stiffness of cancellous bone and as there is also a good correlation between strength and stiffness, it is also a good predictor of strength. In that paper, the authors investigated the ability of ultrasound to predict the mechanical properties of cancellous bone. They found that the speed of sound in cubes of cancellous bone can give structure-specific information and that indeed knowledge of both density and velocity allows for a better prediction of stiffness than either density or velocity alone. Ashman et al. [1], Ashman and Rho [2] used ultrasound to measure the elastic properties of cancellous bone, whereas Fry and Barger [9] used ultrasound to characterize both cortical and cancellous bone.

Moreover, bone rigidity depends to a large extent not only on bone density but also on the trabecular microstructure. This microstructure determines the Biot bone parameters, i.e. they may be determined using homogenization theory.[36–38] Use of Biot's model requires determination of the parameters upon which it depends. This can be an expensive process if done experimentally. In the present paper, we investigate whether these parameters can be ascertained by acoustic interrogation. We revisit the parameter identification problem for two-dimensional bone samples, which we have previously investigated in simplified cases,[27–30,39] the understanding being that this is a predecessor to the full three-dimensional problem.

In Buchanan and Gilbert [27], Buchanan et al. [28], the bone sample was situated in a water tank and we used a boundary element method to model the direct problem and the inversion procedure. The direct problem was solved using a finer mesh size than in the inversion procedure. Some noise was also added to the solution of the direct problem. In these works, simulations were performed for bone specimens of relatively high porosities, and five Biot parameters (porosity β, permeability k, pore size a and real parts of the bulk and shear moduli, Re K_b and Re μ) were determined. The algorithm was uniformly successful in finding the porosity to within 3%. Errors for the remaining parameters were often higher, but the target values of these parameters varied over at least one order of magnitude. The procedure took much CPU time because of the eigenvalues introduced by a finite water tank. The papers [29,30] were an attempt to do away with the water tank and we modelled the problem by replacing the bone sample by an infinite slab. In this case, we were able to numerically compute, to great accuracy, the Green's function for the source in the water using residue calculus. The results were for the most part reasonable; however, inversion

Table 1. Summary of the average and worst errors made by five variants of the inversion algorithm for Problems 71w, …, 91w in Buchanan and Gilbert [30]: Two-phase algorithm with univariate Phase 1; Two-phase algorithm with alternative Phase 1; Three-phase algorithm using the result with the lowest objective function value; Three-phase algorithm using the midpoint of the lowest and highest values; Three-phase algorithm using the mean. See [30] for more details.

Variant	Error	β (%)	k (%)	a (%)	Re K_b (%)	Re μ (%)
Phase 2	Avg.	0.36	10.33	12.13	5.41	7.62
	Worst	1.13	25.75	28.94	17.59	28.59
Phase 2 Alt	Avg.	0.58	15.47	17.54	3.50	4.77
	Worst	2.41	26.09	29.46	6.92	12.42
Phase 3 Obj	Avg.	0.53	13.99	15.50	6.11	7.58
	Worst	2.02	30.24	34.10	17.59	28.59
Phase 3 Mid	Avg.	0.30	12.52	15.87	9.57	9.60
	Worst	0.77	23.41	27.44	23.06	21.86
Phase 3 Mean	Avg.	0.30	12.27	13.31	7.60	8.88
	Worst	0.94	23.52	25.94	21.12	34.73

times were long, ranging from six to nine hours. Table 1 summarizes the results of the various inversion schemes used in Buchanan and Gilbert [30]. More recently, Buchanan et al. [40] investigated an indirect inversion approach based on the numerical solution for a set of effective velocities and transmission coefficients in order to ameliorate the difficulties posed by a direct minimization.

In the present paper, we consider an improved Biot model for orthotropic bone, accounting for dissipation due to tortuosity (i.e. due to the presence of pores of arbitrary size). The bone sample is taken to be a square, and an efficient numerical scheme is devised by adopting a boundary integral formulation for the water tank, so that we need not solve for the entire domain. Only the region occupied by the bone sample is discretized as in Buchanan and Gilbert [27], Buchanan et al. [28], Gilbert et al. [39]. Section 2 presents Biot's model for cancellous bone in the orthotropic and isotropic cases. Section 3 describes the boundary integral formulation for a two-dimensional bone sample immersed in a water tank. Section 4 outlines the numerical scheme to solve the governing equations. Section 5 discusses the inversion results, including convergence and sensitivity tests. Three Biot parameters are examined (porosity, and real parts of the bulk and shear moduli). Finally, concluding remarks are given in Section 6.

2. Biot model for cancellous bone

2.1. *Orthotropic case*

The Biot–Stoll model treats a poroplastic medium as an elastic frame with interspinal pore fluid.[41–43] Cancellous bone is anisotropic; however, as pointed out by Williams [32], if the acoustic waves passing through it travel in the trabecular direction, then an isotropic model may be acceptable. We will simulate a two-dimensional version of the experiments described in McKelvie and Palmer [18] and Hosokawa and Otani [31]. The motions of the frame and fluid within the bone are tracked by position vectors $\mathbf{u} = (u_1, u_2)$ and $\mathbf{U} = (U_1, U_2)$,

respectively. In Cartesian coordinates (x_1, x_2), the two-dimensional constitutive equations relating strain to stress, for an orthotropic material,[44] read

$$\begin{aligned}\sigma_{11} &= \frac{E_1 e_{11} + \nu_1 E_2 e_{22}}{(1-\nu_1\nu_2)} + Q\epsilon,\\ \sigma_{22} &= \frac{\nu_2 E_1 e_{11} + E_2 e_{22}}{(1-\nu_1\nu_2)} + Q\epsilon,\\ \sigma_{12} &= \mu e_{12}, \quad \sigma_{21} = \mu e_{21},\\ s &= Qe + R\epsilon,\end{aligned}$$

where the solid and fluid dilatations are given by

$$e = \nabla\cdot\mathbf{u} = \frac{\partial u_1}{\partial x_1} + \frac{\partial u_2}{\partial x_2}, \qquad \epsilon = \nabla\cdot\mathbf{U} = \frac{\partial U_1}{\partial x_1} + \frac{\partial U_2}{\partial x_2}, \tag{1}$$

and the strains are defined by

$$e_{11} = \frac{\partial u_1}{\partial x_1}, \quad e_{12} = e_{21} = \frac{\partial u_1}{\partial x_2} + \frac{\partial u_2}{\partial x_1}, \quad e_{22} = \frac{\partial u_2}{\partial x_2}. \tag{2}$$

The parameters E_1 and E_2 denote the Young moduli, and ν_1 and ν_2 denote the Poisson ratios, in the x_1- and x_2-directions, respectively. In compliance form, Equations (1) and (2) become

$$\begin{aligned}e_{11} &= -\frac{\nu_2 Q^2\sigma_{22}\nu_1 - \nu_2 Q^2\nu_1\sigma_{11} + \sigma_{22}\nu_1 E_2 R - Q\nu_1 E_2 s - Q^2\sigma_{22} - E_2 R\sigma_{11} + E_2 sQ + Q^2\sigma_{11}}{-Q^2E_1 + RE_2E_1 + \nu_1E_2sQ^2 + Q^2\nu_2E_1E_2 - E_2Q^2},\\ e_{22} &= \frac{-\nu_2Q^2\nu_1\sigma_{11} + \nu_2Q^2\sigma_{22}\nu_1E_1 + Q^2\sigma_{11} - Q^2\sigma_{22} + s\nu_2E_1Q - sE_1Q - R\nu_2\nu_1E_1\sigma_{11} + RE_1\sigma_{22}\nu_2}{-Q^2E_1 + RE_2E_1 + \nu_1E_2Q^2 + Q^2\nu_2E_1 - E_2Q^2},\\ e_{12} &= \frac{\sigma_{12}}{\mu},\\ \epsilon &= \frac{-E_2Q\sigma_{11} + \nu_2E_1Q\sigma_{11}\sigma_{12} + \nu_1E_2Q\sigma_{22} + E_1E_2s - E_1Q\sigma_{22}}{-Q^2E_1 + RE_2E_1 + \nu_1E_2Q^2 + Q^2\nu_2E_1 - E_2e_{11}Q^2}.\end{aligned}$$

Assuming no body forces, an argument based upon Lagrangian dynamics [41,45] leads to the following equations of motion for the displacements and dilatations,

$$\begin{aligned}\left(\mu\mathbb{H}^\top + \frac{1}{1-\nu_1\nu_2}\mathbb{E}\mathbb{H}\right)\mathbf{u} + Q\mathbb{H}\mathbf{U} &= \frac{\partial^2}{\partial t^2}(\rho_{11}\mathbf{u} + \rho_{12}\mathbf{U}) + b\frac{\partial}{\partial t}(\mathbf{u}-\mathbf{U}),\\ \nabla(Qe + R\epsilon) &= \frac{\partial^2}{\partial t^2}(\rho_{12}\mathbf{u} + \rho_{22}\mathbf{U}) - b\frac{\partial}{\partial t}(\mathbf{u}-\mathbf{U}),\end{aligned} \tag{3}$$

where

$$\mathbb{H} := \begin{pmatrix} \frac{\partial^2}{\partial x_1^2} & \frac{\partial^2}{\partial x_1\partial x_2} \\ \frac{\partial^2}{\partial x_1\partial x_2} & \frac{\partial^2}{\partial x_2^2}\end{pmatrix},$$

is the Hessian matrix operator, $\mathbb{H}^\top$ is its transpose and

$$\mathbb{E} := \begin{pmatrix} E_1 & \nu_2E_1 \\ \nu_1E_2 & E_2\end{pmatrix}.$$

Table 2. Parameters in Biot's model for cancellous bone.

Symbol	Parameter
ρ_f	Density of the pore fluid
ρ_r	Density of frame material
K_b	Complex frame bulk modulus
μ	Complex frame shear modulus
K_f	Fluid bulk modulus
K_r	Frame material bulk modulus
β	Porosity
η	Viscosity of pore fluid
Λ	Viscous characteristic length
α_∞	Asymptotic tortuosity
k	Permeability

Here, ρ_{11} and ρ_{22} are density parameters for the solid and fluid, respectively, ρ_{12} is a density coupling parameter, and b is a dissipation parameter. These are calculated from the inputs of Table 2 using the formulas

$$\begin{aligned}\rho_{11} &= (1-\beta)\rho_r - \beta(\rho_f - T\beta),\\ \rho_{12} &= \beta(\rho_f - T\beta),\\ \rho_{22} &= T\beta^2,\end{aligned}$$

where T is the tortuosity. In the time-harmonic case,

$$\mathbf{u}(x_1,x_2,t) = \widehat{\mathbf{u}}(x_1,x_2)e^{i\omega t}, \qquad \mathbf{U}(x_1,x_2,t) = \widehat{\mathbf{U}}(x_1,x_2)e^{i\omega t}.$$

Substituting these representations into (3) and dropping, the hats give

$$\begin{aligned}\left(\mu\mathbb{H}^\top + \frac{1}{1-\nu_1\nu_2}\mathbb{E}\mathbb{H}\right)\mathbf{u} + Q\mathbb{H}\mathbf{U} + \widetilde{p}_{11}\mathbf{u} + \widetilde{p}_{12}\mathbf{U} &= \mathbf{0},\\ \nabla(Qe + R\epsilon) + \widetilde{p}_{12}\mathbf{u} + \widetilde{p}_{22}\mathbf{U} &= \mathbf{0},\end{aligned}$$

where

$$\widetilde{p}_{11} := \omega^2\rho_{11} - i\omega b, \quad \widetilde{p}_{12} := \omega^2\rho_{12} + i\omega b, \quad \widetilde{p}_{22} := \omega^2\rho_{22} - i\omega b.$$

Following Fellah et al. [7,8], an improvement over the standard Biot–Stoll model is obtained by replacing the assumption of cylindrical pores in the dissipation term by a more realistic configuration.[46] This yields

$$\begin{aligned}\left(\mu\mathbb{H}^\top + \frac{1}{1-\nu_1\nu_2}\mathbb{E}\mathbb{H}\right)\mathbf{u} + Q\mathbb{H}\mathbf{U} + p_{11}\mathbf{u} + p_{12}\mathbf{U} &= \mathbf{0},\\ \nabla(Qe + R\epsilon) + p_{12}\mathbf{u} + p_{22}\mathbf{U} &= \mathbf{0},\end{aligned}$$

where

$$p_{11} := \omega^2\Big[(1-\beta)\rho_r + \beta\rho_f(\alpha(\omega)-1)\Big], \; p_{12} := -\omega^2\beta\rho_f(\alpha(\omega)-1), \; p_{22} := \omega^2\beta\rho_f\alpha(\omega),$$

and

$$\alpha(\omega) = \alpha_\infty \left(1 + \frac{i\eta\beta}{\omega\alpha_\infty\rho_f k}\sqrt{1 + \frac{4\alpha_\infty^2 k^2 \rho_f \omega}{i\eta\Lambda^2\beta^2}}\right).$$

It is inconvenient to use both the solid displacement $\mathbf{u}$ and the fluid displacement $\mathbf{U}$ as unknowns. A more convenient set of unknowns are the solid displacement and the pressure $s = Qe + R\epsilon$. To this end, we make the substitutions

$$\mathbf{U} = -\frac{1}{p_{22}}\left(\nabla s + p_{12}\mathbf{u}\right), \quad \epsilon = \frac{1}{R}\left(s - Q\,e\right), \tag{4}$$

to obtain

$$\left(\mu\mathbb{H}^\top + \frac{1}{1-\nu_1\nu_2}\mathbb{E}\mathbb{H} - \frac{p_{12}}{p_{22}}Q\mathbb{H}\right)\mathbf{u} + \left(p_{11} - \frac{p_{12}^2}{p_{22}}\right)\mathbf{u} - \left(\frac{p_{12} + Q\mathbb{H}}{p_{22}}\right)\nabla s = \mathbf{0},$$

and

$$\nabla^2 s + \frac{p_{22}}{R}s + \left(p_{12} - \frac{p_{22}Q}{R}\right)e = 0.$$

This system is well posed under traction boundary conditions. For further details, see the Appendices 1–3.

2.2. *Isotropic case*

Bone is orthotropic; hence, our eventual goal is to investigate parameter retrieval in this case. However, as the problem increases in difficulty with the number of parameters, we first test our procedure on isotropic bone. By assuming isotropy, the constitutive equations simplify to

$$\begin{aligned}\sigma_{11} &= 2\mu e_{11} + \lambda e + Q\epsilon,\\ \sigma_{22} &= 2\mu e_{22} + \lambda e + Q\epsilon,\\ \sigma_{12} &= \mu e_{12}, \quad \sigma_{21} = \mu e_{21}.\end{aligned} \tag{5}$$

It is this case we shall investigate the undetermined coefficient problem for and leave the orthotropic inverse problem for a subsequent publication. The parameter μ, the complex frame shear modulus, is a measured quantity. The other parameters λ, R and Q occurring in the constitutive equations are calculated from the measured or estimated values of the parameters given in Table 2, using the formulas

$$\begin{aligned}\lambda &= K_b - \frac{2}{3}\mu + \frac{(K_r - K_b)^2 - 2\beta K_r(K_r - K_b) + \beta^2 K_r^2}{D - K_b},\\ R &= \frac{\beta^2 K_r^2}{D - K_b},\\ Q &= \frac{\beta K_r\left[(1-\beta)K_r - K_b\right]}{D - K_b},\end{aligned}$$

where

$$D = K_r\Big[1 + \beta(K_r/K_f - 1)\Big].$$

The bulk and shear moduli K_b and μ are often given imaginary parts to account for frame viscoelasticity. Assuming that the bone system oscillates harmonically, Equations (3) become

$$\mu\nabla^2\mathbf{u} + \nabla\Big[(\lambda+\mu)e + Q\epsilon\Big] + (p_{11}\mathbf{u} + p_{12}\mathbf{U}) = \mathbf{0}, \tag{6}$$
$$\nabla(Qe + R\epsilon) + (p_{12}\mathbf{u} + p_{22}\mathbf{U}) = \mathbf{0}.$$

3. Boundary value problem

In a typical *in vitro* experiment, a bone specimen is placed in a water tank. The regions occupied by the bone specimen and the water are denoted by Ω^b and Ω^w, respectively. In Ω^w, the two-dimensional equations for fluid pressure P and fluid displacement $\mathbf{U}^w = (U_1^w, U_2^w)$ read

$$-\nabla^2 P - k_0^2 P = -q\,\delta(\mathbf{x};\mathbf{x}_0;k_0), \tag{7}$$
$$\nabla P - \rho^w\omega^2\mathbf{U}^w = \mathbf{0}, \tag{8}$$

where ρ^w is the water density, $\mathbf{x}_0$ is the location of the point source, q and k_0 are the amplitude and wavenumber of the emitted signal, respectively. As stated above, in order to formulate a well-posed boundary value problem, one must modify the present form of Biot's Equation (6), since there are not enough transmission conditions for the components of displacements fields $\mathbf{u}$ and $\mathbf{U}$. Using s as defined in (4), we obtain

$$\nabla^2 s + \frac{p_{22}}{R}s + \left(p_{12} - \frac{p_{22}Q}{R}\right)e = 0, \tag{9}$$

together with

$$\mu\nabla^2\mathbf{u} + \nabla\Big[\Big(\lambda+\mu-\frac{Q^2}{R}\Big)e + \Big(\frac{Q}{R} - \frac{p_{12}}{p_{22}}\Big)s\Big] + \Big(p_{11} - \frac{p_{12}^2}{p_{22}}\Big)\mathbf{u} = \mathbf{0}. \tag{10}$$

Equations (9) and (10) then form the modified Biot equations for $\mathbf{u}$ and s in the bone specimen Ω^b. These equations should be satisfied by $\mathbf{u}$ and s together with boundary conditions on the interface between bone and water. These are:

- Continuity of the flux: from (8), we have

$$\rho^w\omega^2\Big[\beta\mathbf{n}\cdot\mathbf{U} + (1-\beta)\mathbf{n}\cdot\mathbf{u}\Big] = \rho^w\omega^2\mathbf{n}\cdot\mathbf{U}^w \equiv 0,$$

  and thus

$$\rho^w\omega^2\left(\Big[1-\beta\Big(1+\frac{p_{12}}{p_{22}}\Big)\Big]\mathbf{n}\cdot\mathbf{u} - \frac{\beta}{p_{22}}\frac{\partial s}{\partial n}\right) = 0, \tag{11}$$

  where $\mathbf{n}$ is the exterior unit normal to Ω^b, pointing into the water.
- Continuity of the aggregate pressure:

$$\sigma_{\ell j}\,n_j + s\,n_\ell = -Pn_\ell, \tag{12}$$

  since an expansion of the bone induces a compression in the water.
- Continuity of the pore pressure:

$$s = -\beta P. \tag{13}$$

- Vanishing of the tangential frame stress: $\sigma_{12} \equiv \sigma_{21} = 0$ which is equivalent to

$$\frac{\partial u_1}{\partial x_2} + \frac{\partial u_2}{\partial x_1} = 0. \tag{14}$$

In addition, it is understood that the pressure P is also required to satisfy the two-dimensional Sommerfeld radiation condition at infinity. We have so far given the precise formulation of the exterior transmission problem (ETP) consisting of Equations (9), (10) for the unknowns $\mathbf{u}, s$ in Ω^b and Equation (7) for the unknown P in Ω^w, together with transmission conditions (11)–(14) and the radiation condition at infinity.

From the computational point of view, it is more convenient to reduce the ETP to a nonlocal problem in a finite computational domain such as Ω^b.[39] For this purpose, we now reduce the Helmholtz Equation (7) to a boundary integral equation using the Green representation of P in Ω^w. More precisely, we seek a solution of (7) in the form of a single-layer potential in terms of the unknown density function φ,

$$P(\mathbf{x}, \mathbf{x}_0) = -q\, G(\mathbf{x}, \mathbf{x}_0; k_0) - \int_{\partial\Omega^b} G(\mathbf{x}, \zeta; k_0)\varphi(\mathbf{x}_0, \zeta)\, dS_\zeta, \quad \mathbf{x} \in \Omega^w,$$

where $G(\mathbf{x}, \mathbf{x}_0, k_0)$ is free-space Helmholtz Green's function given by

$$G(\mathbf{x}, \mathbf{x}_0, k_0) := \frac{i}{4} H_0^{(1)}(k_0\|\mathbf{x} - \mathbf{x}_0\|),$$

and $H_0^{(1)}$ is a Hankel function of the first kind. Clearly, the density function φ is related to the unknowns $\mathbf{u}$ and $\mathbf{U}$ via the transmission conditions (11)–(14).

If the boundary $\partial\,\Omega^b$ of the bone sample has positive orientation, then letting $\mathbf{x} \to \mathbf{X} \in \partial\,\Omega^b$, we obtain from condition (12) that

$$\lambda\nabla\cdot\mathbf{u} + 2\mu\frac{\partial u_1}{\partial x_1} + Q\epsilon + s = q\, G(\mathbf{X}, \mathbf{x}_0; k_0) + \int_{\partial\Omega^b} G(\mathbf{X}, \zeta; k_0)\varphi(\mathbf{x}_0, \zeta)\, ds_\zeta, \tag{15}$$

and

$$\lambda\nabla\cdot\mathbf{u} + 2\mu\frac{\partial u_2}{\partial x_2} + Q\epsilon + s = q\, G(\mathbf{X}, \mathbf{x}_0; k_0) + \int_{\partial\Omega^b} G(\mathbf{X}, \zeta; k_0)\varphi(\mathbf{x}_0, \zeta)\, ds_\zeta. \tag{16}$$

Note that in deriving these equations, we have tacitly employed condition (14). In view of the similarity between (15) and (16), a subtraction of these two equations leads to the simple relation

$$\frac{\partial u_1}{\partial x_1} - \frac{\partial u_2}{\partial x_2} = 0. \tag{17}$$

Hence in computation, we may use (17) and either (15) or (16), but not both. Here, the term ϵ should be replaced by $\epsilon = (s - Q\,e)/R$ from (4).

Next, the flux continuity condition (11) leads to the natural boundary condition for s,

$$\begin{aligned}\rho^w\omega^2\left(\left[1 - \beta\left(1 + \frac{p_{12}}{p_{22}}\right)\right]\mathbf{n}\cdot\mathbf{u} - \frac{\beta}{p_{22}}\frac{\partial s}{\partial n}\right) + q\,\frac{\partial G}{\partial n}(\mathbf{X}, \mathbf{x}_0; k_0)\\ = \frac{1}{2}\varphi(\mathbf{x}_0, \mathbf{X}) - \int_{\partial\,\Omega^b}\varphi(\mathbf{x}_0, \zeta)\frac{\partial G}{\partial n}(\mathbf{X}, \zeta; k_0)\, ds_\zeta.\end{aligned} \tag{18}$$

Note that the normal derivatives of G in (18) are taken with respect to $\mathbf{X}$. Finally, from the representation formula for P, condition (13) leads to a boundary integral equation for φ,

$$\beta \int_{\partial\Omega^b} G(\mathbf{X}, \zeta; k_0)\varphi(\mathbf{x}_0, \zeta)\, \mathrm{d}s_\zeta - s + \beta\, q\, G(\mathbf{X}, \mathbf{x}_0; k_0) = 0. \tag{19}$$

It is worth mentioning that the right-hand sides of (15), (16), (18) and (19) contain no singularities since, for the first three equations, the source point $\mathbf{x}_0$ is in Ω^b whereas, for (18), the singularity is cancelled because of the last term on the right-hand side.

Before we formulate what is called *the nonlocal problem* for the ETP, some observations are in order. We observe that the transmission conditions (15) and (16) can be considered as

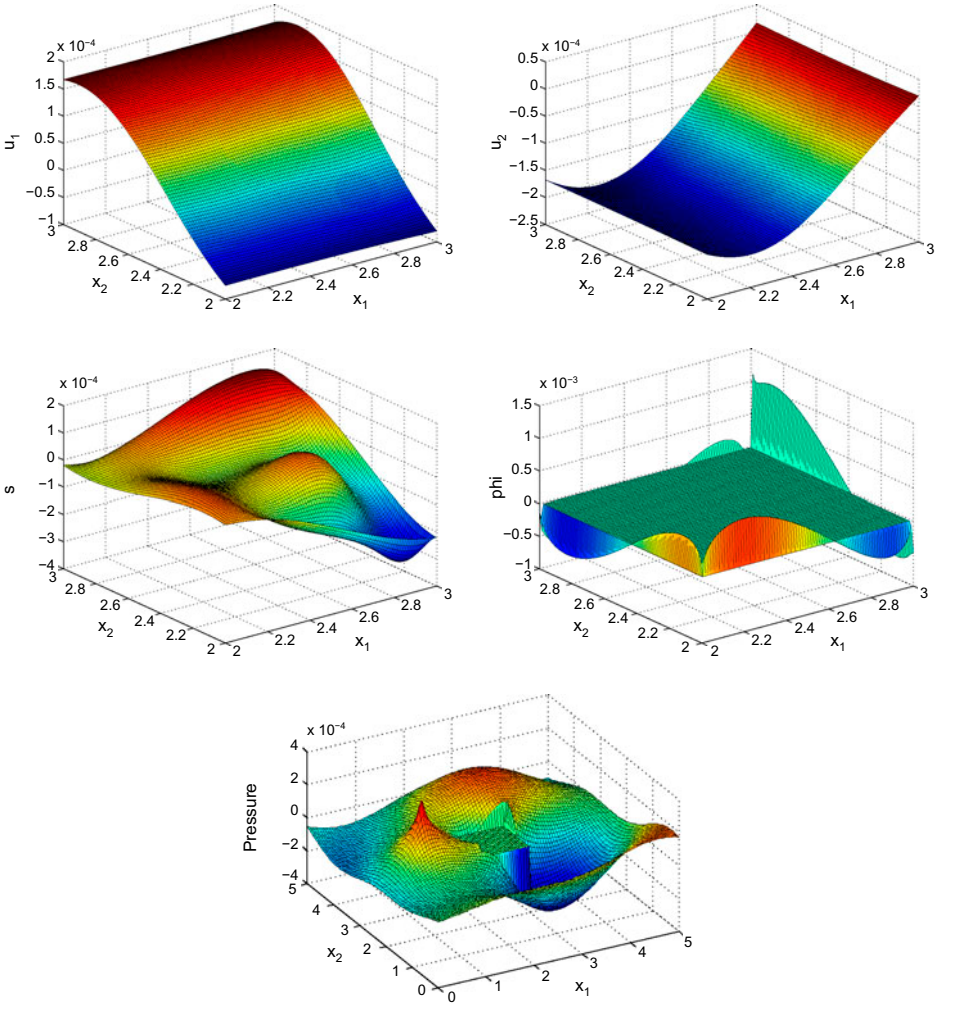

Figure 1. Profiles of u_1, u_2, s, φ and $-P$ for $N = 90$, $\omega = 250\,\mathrm{kHz}$ and $\beta = 0.7$.

natural boundary conditions for the displacement field **u** for given s and φ, whereas condition (18) is a natural condition for the stress s if **u** and φ are known. From the variational point of view, both equations define the relevant Dirichlet–Neumann maps. On the other hand, condition (19) only relates the trace of the stress s and the density function φ, which may be considered as a boundary integral equation for φ given the stress s. With these observations, we are now in a position to state the nonlocal problem for the ETP:

Find the four unknowns u_1, u_2, s, φ. The first three unknowns are required to satisfy the Biot Equations (9) and (10) *and the boundary conditions* (or rather the transmission

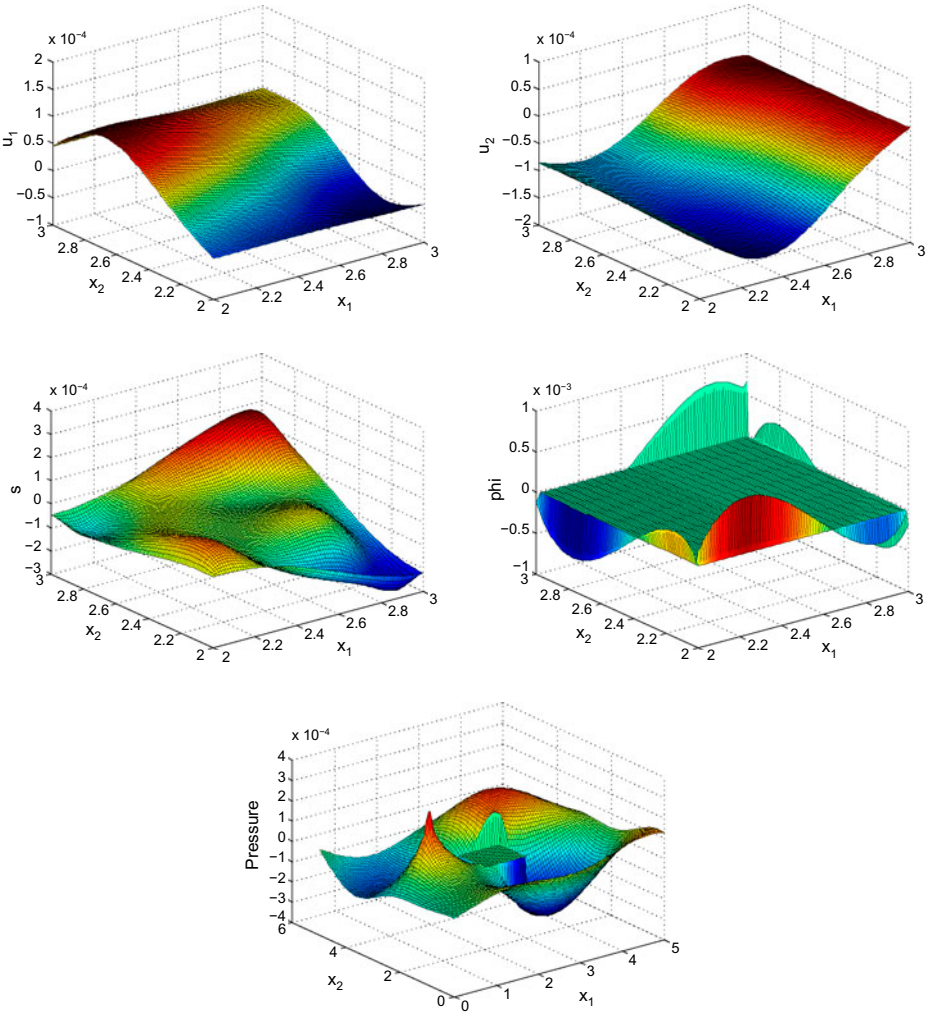

Figure 2. Profiles of u_1, u_2, s, φ and $-P$ for $N = 90$, $\omega = 250\,\text{kHz}$ and $\beta = 0.83$.

conditions) *either* (15) *or* (16), (17) *and* (18), *where the density function* φ *may be considered as an unknown parameter subject to the constraint* (19).

We note that if φ is given, then we have an uncoupled system for the displacement components u_1, u_2 and stress s. On the other hand, if u_1, u_2 and s are given, then the unknown density function φ is required to satisfy the standard Fredholm boundary integral equation of the first kind (19). In general, this is a coupled system for the four unknowns, and can only be treated by numerical methods, which is the content of the next section.

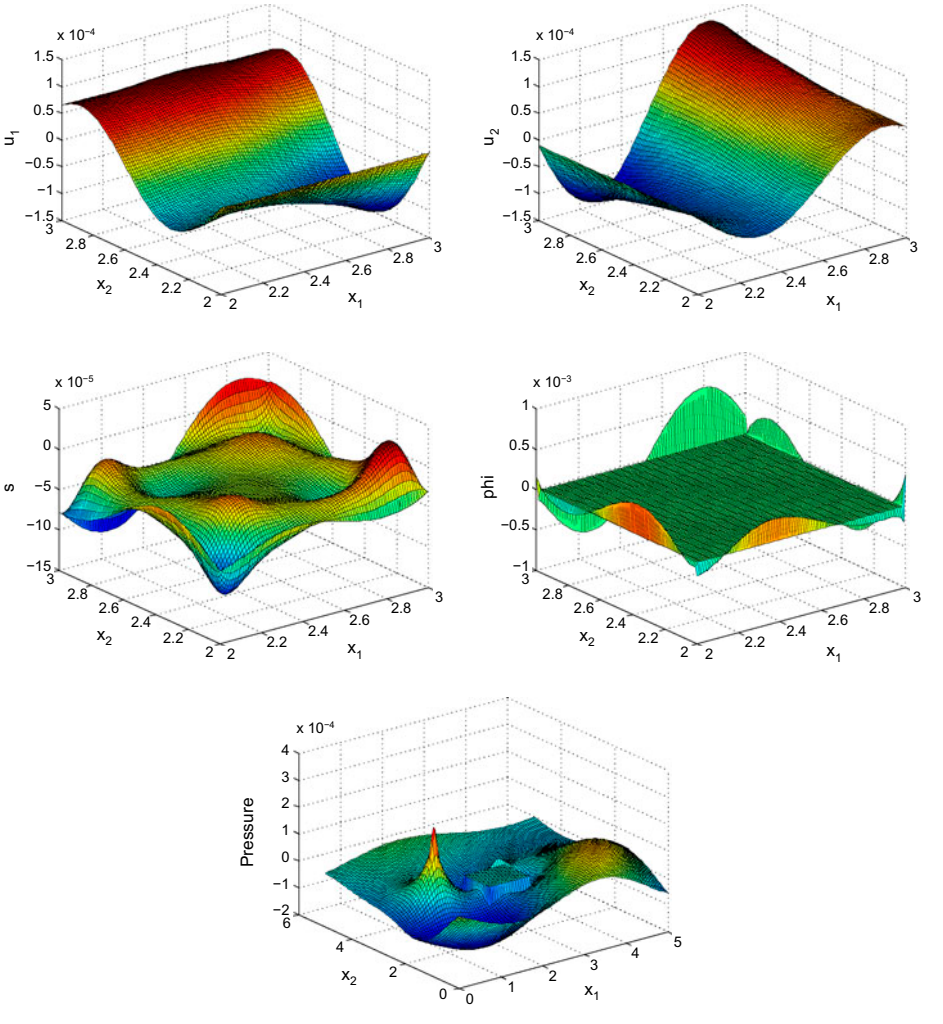

Figure 3. Profiles of u_1, u_2, s, φ and $-P$ for $N = 90$, $\omega = 250\,\text{kHz}$ and $\beta = 0.9$.

4. Numerical approximation

In this section, we will assume that the bone specimen is a square of dimension $L \times L$. We discretize the domain into a uniform mesh consisting of $N \times N$ points. In order to solve the coupled system of Equations (9), (10), (15) or (16)–(19), we use a finite-difference method.

The discretization of derivatives is carried out in the following way: second-order central difference schemes are used for the bulk equations, and either backward or forward second-order schemes are used for the boundary conditions depending on the node location. Tangential derivatives along the boundary are discretized using only first-order backward schemes. The reason for this is to avoid special treatment of boundary nodes in order to keep implementation of the finite-difference method relatively simple. Finally, the quadrature of

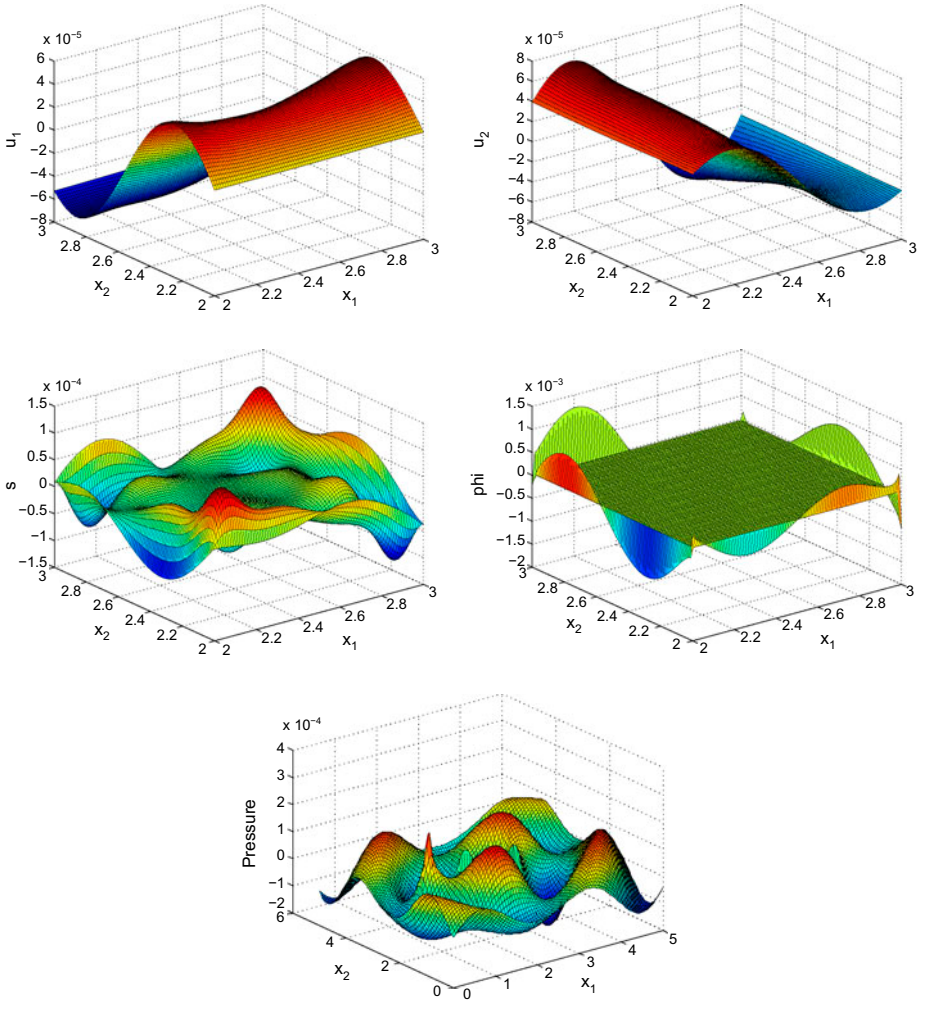

Figure 4. Profiles of u_1, u_2, s, φ and $-P$ for $N = 90$, $\omega = 500\,\text{kHz}$ and $\beta = 0.7$.

the boundary integrals in (15) or (16), (18) and (19) is based on constant interpolation of the solution between grid points. The resulting system is then solved by Gaussian elimination. For instance, following this scheme and using the appropriate standard finite-difference formulas

$$\frac{\partial f}{\partial x}(x_i, y_j) \approx \frac{-3f_{i,j} + 4f_{i+1,j} - f_{i+2,j}}{2h}, \quad \text{(forward)}$$
$$\frac{\partial f}{\partial x}(x_i, y_j) \approx \frac{f_{i-2,j} - 4f_{i-1,j} + 3f_{i,j}}{2h}, \quad \text{(backward)}$$

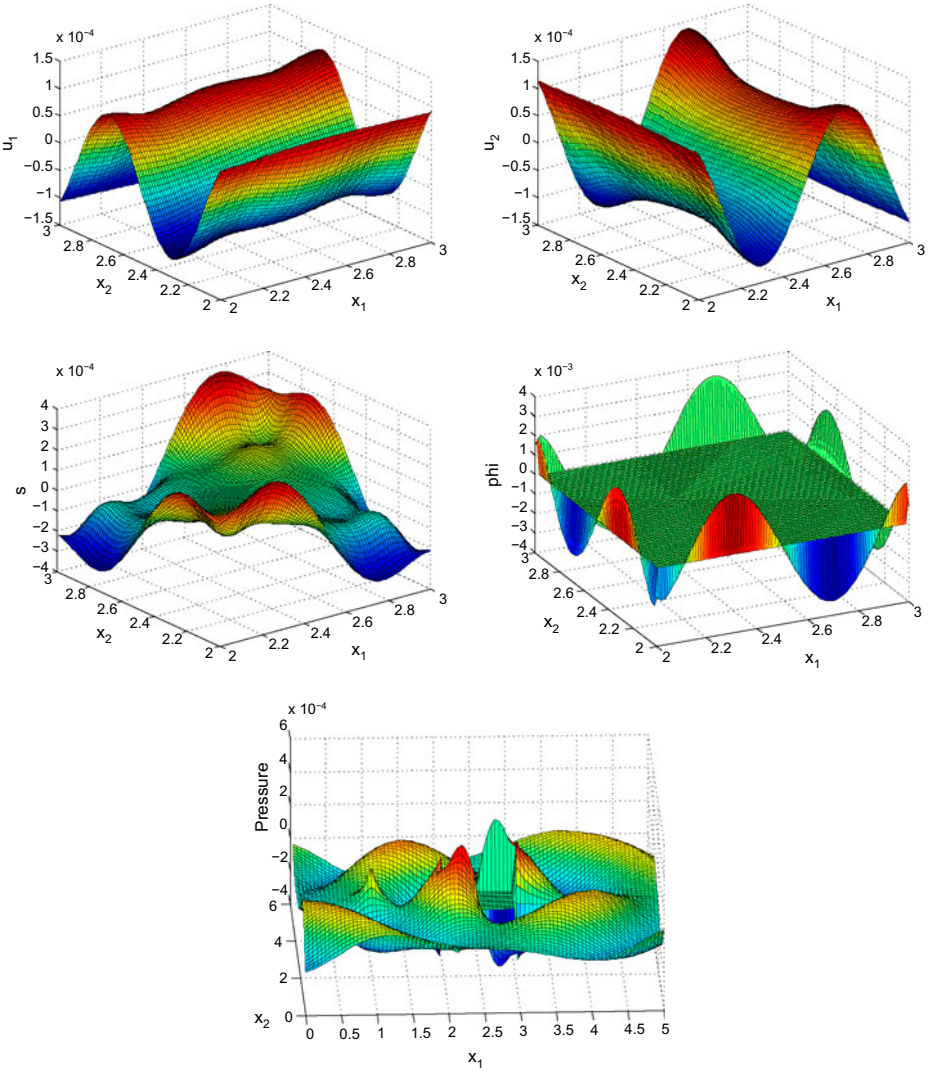

Figure 5. Profiles of u_1, u_2, s, φ and $-P$ for $N = 90$, $\omega = 500\,\text{kHz}$ and $\beta = 0.83$.

$$\frac{\partial^2 f}{\partial x^2}(x_i, y_j) \approx \frac{f_{i-1,j} - 2f_{i,j} + f_{i+1,j}}{h^2},$$
$$\frac{\partial^2 f}{\partial x \partial y}(x_i, y_j) \approx \frac{f_{i+1,j+1} - f_{i+1,j-1} + f_{i-1,j-1} - f_{i-1,j+1}}{4h^2},$$

Equation (16) on the left side of the square away from the corners becomes

$$\left(\lambda + 2\mu - \frac{Q^2}{R}\right)\left(-3u1_{(i,j)} + 4u1_{(i+1,j)} - u1_{(i+2,j)}\right) + 2\left(\lambda - \frac{Q^2}{R}\right)\left(u2_{(i,j)} - u2_{(i,j-1)}\right)$$
$$+ 2h\left(1 + \frac{Q}{R}\right)s_{(i,j)} - 2h^2 \sum_{\zeta_{(m,n)} \in \partial\Omega^b} G(\mathbf{X}_{(i,j)}, \zeta_{(m,n)}; k_0)\varphi(\mathbf{x}_0, \zeta_{(m,n)}) = 2h\, q\, G(\mathbf{X}_{(i,j)}, \mathbf{x}_0; k_0).$$

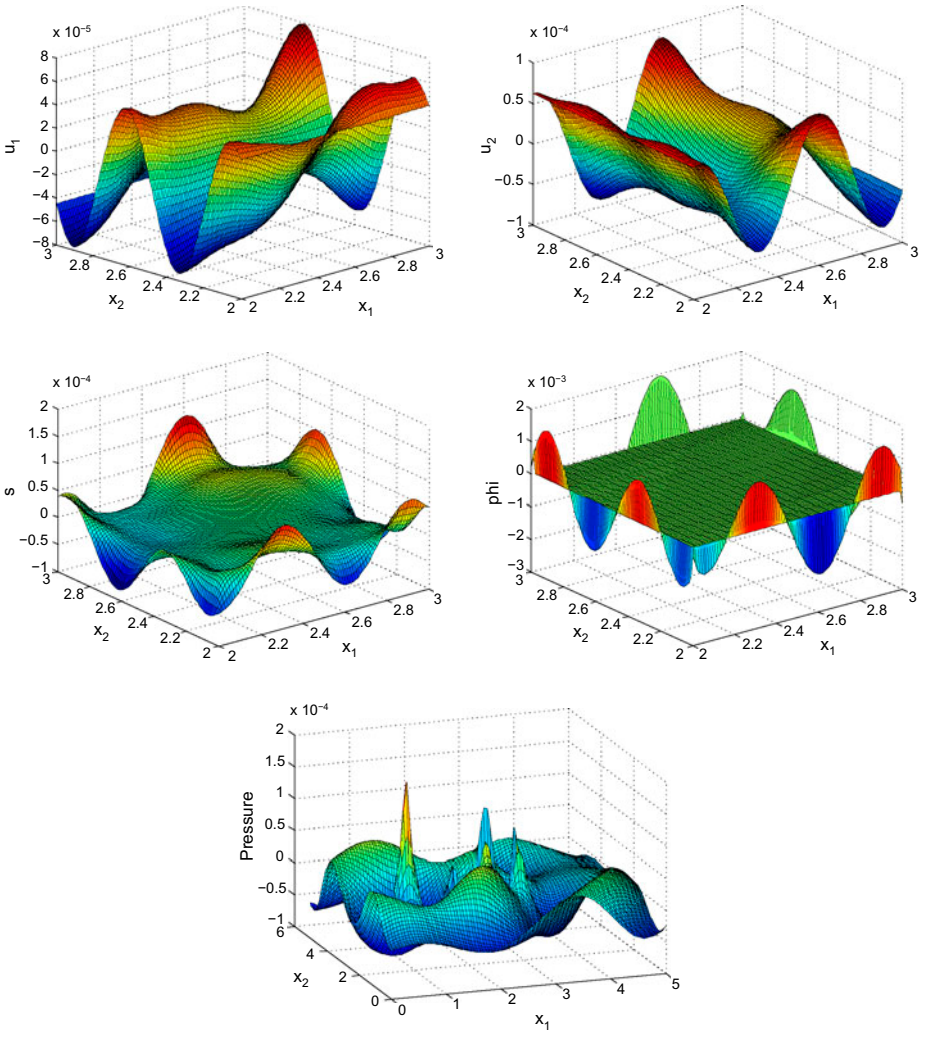

Figure 6. Profiles of u_1, u_2, s, φ and $-P$ for $N = 90$, $\omega = 500\,\text{kHz}$ and $\beta = 0.9$.

Table 3. Convergence test on β with the NM algorithm for varying resolutions and $\eta = \eta_1$.

ω	low/high	β	$f_{\min}$	% error
Guess/Target		0.7		
250 kHz	25/90	0.6945	0.3671	0.7857
	45/90	0.6940	0.1654	0.8571
	65/90	0.6971	0.0697	0.4142
Guess/Target		0.7		
500 kHz	25/90	0.7345	0.2366	4.929
	45/90	0.7172	0.1171	2.443
	65/90	0.7081	0.0486	1.157
Guess/Target		0.83		
250 kHz	25/90	0.8350	0.3014	0.6024
	45/90	0.8304	0.1178	0.0602
	65/90	0.8298	0.0439	0.0241
Guess/Target		0.83		
500 kHz	25/90	0.8581	0.4467	3.389
	45/90	0.8406	0.2174	1.277
	65/90	0.8343	0.0865	0.5181
Guess/Target		0.9		
250 kHz	25/90	0.8844	0.7037	1.733
	45/90	0.8993	0.3412	0.0778
	65/90	0.9015	0.1162	0.1667
Guess/Target		0.9		
500 kHz	25/90	0.9437	0.2791	4.855
	45/90	0.9040	0.0992	0.4444
	65/90	0.9020	0.0799	0.2222

Here,

$$G(\mathbf{X}, \zeta; k_0) = \begin{cases} \dfrac{i}{4} H_0^{(1)}(k_0 \|\mathbf{X} - \zeta\|), & \mathbf{X} \neq \zeta, \\ \dfrac{i}{8\pi} h \left[\log\left(\dfrac{2}{h}\right) + 1 \right], & \mathbf{X} = \zeta, \end{cases}$$

and h is the mesh spacing.

Before proceeding with numerical tests for this model, as an illustration, Figures 1–6 show dimensionless profiles of u_1, u_2, s (in Ω^b), φ (on $\partial\Omega^b$) and $-P$ (in Ω^w), using $L = 1$ and $N = 90$, for various frequencies ω and porosities β. Values of physical parameters used in these numerical simulations are given in the next section. We restrict ourselves to relatively low ultrasonic frequencies, 250 and 500 kHz, where Biot's model is supposed to be applicable. Moreover, in view of applications to quantitative ultrasound techniques for the diagnosis of osteoporosis, we pay particular attention to relatively high bone porosities.

5. Numerical experiments

5.1. *Convergence/accuracy tests*

To validate our model, we perform several tests using different optimization procedures. These are the Nelder–Mead (NM) simplex algorithm and the Differential Evolution (DE)

Table 4. Convergence test on β with the NM algorithm for varying resolutions and $\eta = \eta_2$.

ω	low/high	β	$f_{\min}$	% error
Guess/Target		0.7		
250 kHz	25/90	0.6944	0.1879	0.800
	45/90	0.6944	0.0871	0.800
	65/90	0.6973	0.0374	0.3857
Guess/Target		0.7		
500 kHz	25/90	0.7711	0.2949	10.157
	45/90	0.7405	0.1284	5.786
	65/90	0.7201	0.0485	2.871
Guess/Target		0.83		
250 kHz	25/90	0.9019	0.9753	8.663
	45/90	0.9054	0.9556	9.084
	65/90	0.8276	0.2619	0.2891
Guess/Target		0.83		
500 kHz	25/90	0.8476	0.4707	2.120
	45/90	0.8389	0.2729	1.072
	65/90	0.8338	0.1327	0.4578
Guess/Target		0.9		
250 kHz	25/90	0.9030	0.3626	0.333
	45/90	0.9031	0.1363	0.3444
	65/90	0.9020	0.0514	0.2222
Guess/Target		0.9		
500 kHz	25/90	0.8990	0.2912	0.1111
	45/90	0.8998	0.1329	0.0222
	65/90	0.8999	0.0567	0.0111

scheme. As in Buchanan and Gilbert [30], to implement the NM algorithm, we use the MATLAB command *fminsearch*. A MATLAB code for the DE scheme can be found at http://www1.icsi.berkeley.edu/~storn/code.html. To our knowledge, this is the first time that DE is applied to the present context.

Before we discuss our numerical experiments, let us briefly describe these two derivative-free optimization methods. The fact that there is no derivative data needed to use these algorithms makes them applicable to a wide variety of problems. However, this type of optimization methods also has significant drawbacks. The DE scheme is an example of a population-based stochastic search method that is used for global optimization. One very appealing feature of this scheme is that very little user input is required. For instance, unlike the NM algorithm, no initial guess is needed to start the search with DE. This is a particularly salient feature since it has the effect of being able to stimulate some level of uncertainty in determining the parameters of cancellous bone. More specifically, to find an accurate minimum using the NM algorithm, one must have an accurate guess in the first place, otherwise it may converge to a local minimum. The DE scheme eliminates any bias in this regard. The main drawback of evolutionary algorithms is that, depending on the cost function, convergence may be slow.[47] For more information regarding the DE scheme, see [48]. The NM algorithm is another example of a direct search method, which can be

Table 5. Comparison test on β between $RN = 11$ and $RN = 100$ for $\eta = \eta_1$. Here $N = 50$ for the high resolution and $N = 25$ for the low resolution.

ω	β	$f_{\min}$	% error
Guess/Target	0.7		
250 kHz			
11 Receiving nodes	0.7032	0.2692	0.4571
100 Receiving nodes	0.7035	0.2690	0.5000
Guess/Target	0.7		
500 kHz			
11 Receiving nodes	0.7252	0.1318	3.600
100 Receiving nodes	0.7252	0.1290	3.600
Guess/Target	0.83		
250 kHz			
11 Receiving nodes	0.8345	0.2124	0.5422
100 Receiving nodes	0.8345	0.2164	0.5422
Guess/Target	0.83		
500 kHz			
11 Receiving nodes	0.8504	0.3870	2.458
100 Receiving nodes	0.8504	0.3865	2.458
Guess/Target	0.9		
250 kHz			
11 Receiving nodes	0.8898	0.5700	1.133
100 Receiving nodes	0.8897	0.5645	1.144
Guess/Target	0.9		
500 kHz			
11 Receiving nodes	0.9033	0.1118	0.3667
100 Receiving nodes	0.9034	0.1142	0.3777

applied to a wide variety of cost functions, just as with DE. Since a starting guess must be supplied to initiate the algorithm, convergence to a global minimum may not occur, especially if the cost function has many minima. It is for this reason that we compare the NM and DE results, since the latter may be more successful at finding the global minimum. Moreover, the NM algorithm may not be desirable to use for problems with many variables to be determined (as shown in Nelder and Mead [49]) and, in higher dimensions, there is a large number of function evaluations needed for convergence. This can be very time intensive especially when the cost function is complicated. For further details on the NM algorithm and its convergence properties, we refer the reader to [49,50].

We now discuss our numerical experiments. For a given value of β, we may calculate the pressure at a certain number RN of receiving nodes outside of the bone specimen. We do this for two different resolutions to compare the results. For our tests, we assume that the centre of the square is located at $(5L/2, 5L/2)$, and that the source is positioned at $\mathbf{x}_0 = (L, 5L/2)$ outside of the square. The physical parameters we specify are (in dimensional SI units): $L = 0.01$, $\rho_f = 950$, $\rho_r = 1960$, $K_f = 2 \times 10^9$, $K_r = 2 \times 10^{10}$, $a_\infty = 1.13$ and $\Lambda = 5 \times 10^{-6}$. In order to see if the model can handle changes in physical parameters, we

Table 6. Comparison test on β between $RN = 11$ and $RN = 100$ for $\eta = \eta_2$. Here, $N = 50$ for the high resolution and $N = 25$ for the low resolution.

ω	β	$f_{\min}$	% error
Guess/Target	0.7		
250 kHz			
11 Receiving nodes	0.6983	0.1096	0.2429
100 Receiving nodes	0.6989	0.1118	0.1571
Guess/Target	0.7		
500 kHz			
11 Receiving nodes	0.7513	0.1542	7.329
100 Receiving nodes	0.7514	0.1555	7.343
Guess/Target	0.83		
250 kHz			
11 Receiving nodes	0.9044	0.985	8.964
100 Receiving nodes	0.9043	0.9845	8.952
Guess/Target	0.83		
500 kHz			
11 Receiving nodes	0.8407	0.3091	1.289
100 Receiving nodes	0.8407	0.3098	1.289
Guess/Target	0.9		
250 kHz			
11 Receiving nodes	0.9029	0.2592	0.3222
100 Receiving nodes	0.9029	0.2551	0.3222
Guess/Target	0.9		
500 kHz			
11 Receiving nodes	0.8998	0.1911	0.0222
100 Receiving nodes	0.8999	0.1980	0.0111

use two different values for η, $\eta_1 = 1.5$ (blood marrow) and $\eta_2 = 0.001$ (water), thus each set of numerical tests is performed twice.

To begin our numerical testing, let P_ℓ^* represent the pressure at point $\mathbf{x}_\ell = (x_i, y_j)$. Trial values P_ℓ produced by a set of Biot parameters are compared to the values P_ℓ^* using the objective function

$$f(P_\ell, P_\ell^*) = \frac{\left[\sum_{\ell=1}^{RN}(P_\ell^* - P_\ell)^2\right]^{1/2}}{\left[\sum_{\ell=1}^{RN}(P_\ell^*)^2\right]^{1/2}}. \tag{20}$$

For our first test, we compare varying sets of resolutions. We are interested in determining the value of β that minimizes the objective function (20), with $f_{\min}$ denoting this minimum. The minimization procedure is done using the NM simplex algorithm. We use the lower resolutions $N = (25, 45, 65)$ to produce the trial values, and compare these to the higher resolution $N = 90$. Due to limitations in computing resources, simulations with resolutions higher than $N = 90$ were prohibitive. For this test, the pressure is calculated at $RN = 11$

Table 7. Comparison test on β between $RN = 11$ and $RN = 100$ for $\eta = \eta_1$. Here, $N = 50$ for the high resolution and $N = 25$ for the low resolution. Receiving nodes are placed near the top, bottom and to the right of the bone sample.

ω	β	$f_{\min}$	% error
Guess/Target	0.7		
250 kHz			
11 Receiving nodes	0.6998	0.2555	0.0286
100 Receiving nodes	0.6999	0.2554	0.0143
Guess/Target	0.7		
500 kHz			
11 Receiving nodes	0.7269	0.1739	3.840
100 Receiving nodes	0.7269	0.1735	3.840
Guess/Target	0.83		
250 kHz			
11 Receiving nodes	0.8342	0.1323	0.5060
100 Receiving nodes	0.8342	0.1323	0.5060
Guess/Target	0.83		
500 kHz			
11 Receiving nodes	0.8500	0.3708	2.4096
100 Receiving nodes	0.8499	0.3698	2.4000
Guess/Target	0.9		
250 kHz			
11 Receiving nodes	0.8928	0.5111	0.8000
100 Receiving nodes	0.8929	0.5077	0.7889
Guess/Target	0.9		
500 kHz			
11 Receiving nodes	0.9040	0.0912	0.4444
100 Receiving nodes	0.9041	0.0903	0.4560

receiving points outside the square, opposite to the source. These points are evenly spaced in the interval $x_1 = 4L$ and $L \leq x_2 \leq 4L$. The stopping criterion that we imposed in the minimization depends on the scheme. For the NM algorithm, we typically used the default criterion in *fminsearch*. For the stopping criterion in the DE scheme as discussed later, we specified a maximum of 150 iterations. Our choice of 150 iterations was based on experimental observations. We can see from the results in Tables 3 and 4 that the numerical scheme does appear to converge and that, in most cases, our guess for β is quite accurate. We also mention that there does appear to be good frequencies and bad frequencies to use for the purpose of obtaining numerical data.

For our next test, we determine if increasing the number of measurement points RN will make our results more accurate. We compare the results for $RN = 11$ to those for $RN = 100$ (distributed over the same interval $x_1 = 4L$, $L \leq x_2 \leq 4L$). Due to the larger number of constraints for $RN = 100$, computations were found to be more demanding in CPU time. Therefore, to carry out this test, we use $N = 50$ for the high resolution and $N = 25$ for the low resolution. From Tables 5 to 6, we can see that there is no significant change in results when we take more receiving nodes. However, placement of nodes may

Table 8. Comparison test on β between $RN = 11$ and $RN = 100$ for $\eta = \eta_2$. Here, $N = 50$ for the high resolution and $N = 25$ for the low resolution. Receiving nodes are placed near the top, bottom and to the right of the bone sample.

ω	β	$f_{\min}$	% error
Guess/Target	0.7		
250 kHz			
11 Receiving nodes	0.6884	0.0618	1.657
100 Receiving nodes	0.6885	0.0620	1.643
Guess/Target	0.7		
500 kHz			
11 Receiving nodes	0.7465	0.1699	6.643
100 Receiving nodes	0.7464	0.1716	6.629
Guess/Target	0.83		
250 kHz			
11 Receiving nodes	0.9076	0.9937	9.350
100 Receiving nodes	0.9076	0.9937	9.350
Guess/Target	0.83		
500 kHz			
11 Receiving nodes	0.8396	0.2685	1.157
100 Receiving nodes	0.8396	0.2679	1.157
Guess/Target	0.9		
250 kHz			
11 Receiving nodes	0.9046	0.2252	0.5111
100 Receiving nodes	0.9046	0.2234	0.5111
Guess/Target	0.9		
500 kHz			
11 Receiving nodes	0.8979	0.0842	0.2333
100 Receiving nodes	0.8980	0.0854	0.2222

have an effect on numerical data. As an additional test, we place evenly spaced receiving nodes at $5L/2 \leq x_1 \leq 4L$, $x_2 = 4L$ near the top of the square, at $5L/2 \leq x_1 \leq 4L$, $x_2 = L$ near the bottom of the square and nodes to the right of the square at $x_1 = 4L$, $2L \leq x_2 \leq 3L$. Both cases $RN = 11$ and $RN = 100$ are examined. Again, from Tables 7 to 8, we see that there is no much difference when we alter the placement of the measurement points. Therefore, for convenience in the following tests, we will use $RN = 11$ receiving nodes evenly placed to the right of the bone sample, at $x_1 = 4L$ and $L \leq x_2 \leq 4L$.

Next, we minimize the objective function (20) using the DE scheme and compare these results to the values obtained by minimizing with the NM algorithm. Here again, we take $N = 25$ for the low resolution and $N = 50$ for the high resolution. Tables 9 and 10 indicate that the NM minimum agrees with the DE one in most cases, which suggests that our model is robust in particular with respect to the minimization procedure.

Finally, we perform a sensitivity test on the determination of β. In this case, a target high-resolution ($N = 90$) simulation is performed for a given value of β and compared with trial low-resolution ($N = 65$) simulations for a range of values of β. The comparison is based on a direct evaluation of the objective function (20) without minimization. These

Table 9. Comparison between the NM and DE minima for $\eta = \eta_1$. Here, $N = 50$ for the high resolution and $N = 25$ for the low resolution.

ω	β	$f_{\min}$	% error
Guess/Target	0.7		
250 kHz			
NM	0.7032	0.2692	0.4571
DE	0.7032	0.2692	0.4571
Guess/Target	0.7		
500 kHz			
NM	0.7252	0.1318	3.600
DE	0.7252	0.1318	3.600
Guess/Target	0.83		
250 kHz			
NM	0.8345	0.2124	0.5422
DE	0.8345	0.2124	0.5422
Guess/Target	0.83		
500 kHz			
NM	0.8504	0.3870	2.458
DE	0.8504	0.3870	2.458
Guess/Target	0.9		
250 kHz			
NM	0.8898	0.5700	1.133
DE	0.8898	0.5700	1.133
Guess/Target	0.9		
500 kHz			
NM	0.9033	0.1118	0.3667
DE	0.9033	0.1118	0.3667

results are presented in Figures 7 and 8 and show that the minimum of the objective function occurs near the target value of β in all cases. This is consistent with the findings from our previous tests, and further supports the robustness of our model.

These preliminary results are encouraging in regards to trying to recover other parameters by this approach, and suggest that we may have some success at recovering additional parameters. After the minimization procedure is carried out, we can use our guess for β to determine guesses for other parameters. In particular, this value allows us to calculate guess values for the following parameters: Re K_b, and Re μ. We can obtain these guesses using the following formulas in terms of β:

- The real parts of K_b and μ are calculated by the formulas of Williams [32],

$$\begin{aligned} \operatorname{Re} K_b &= \frac{E}{3(1-2\nu)} V_f^n, \\ \operatorname{Re} \mu &= \frac{E}{2(1+\nu)} V_f^n, \end{aligned} \tag{21}$$

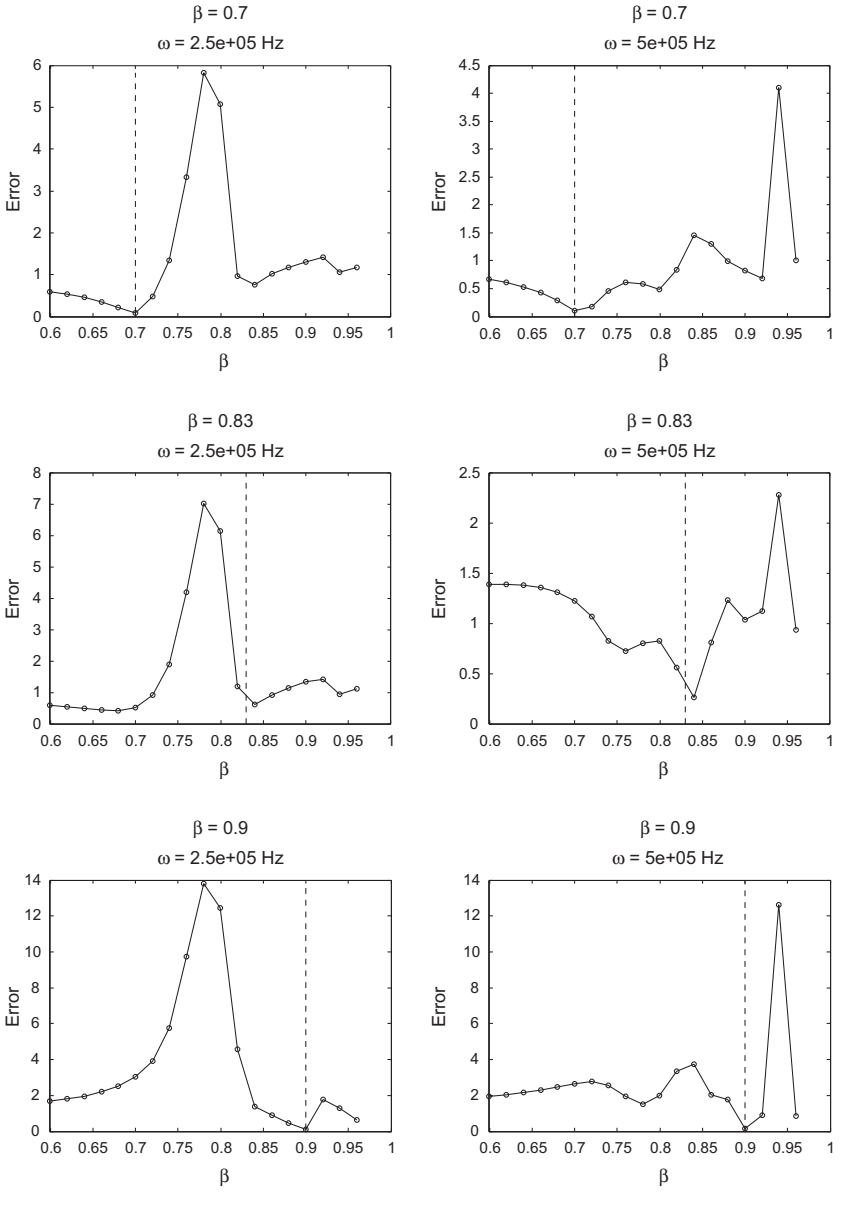

Figure 7. Sensitivity test on β for $\eta = \eta_1$. Here, $N = 90$ for the high resolution and $N = 65$ for the low resolution. The vertical dashed line corresponds to the target value of β specified in the high-resolution simulation. Both frequencies 250 and 500 kHz are considered.

where $V_f = 1 - \beta$ is the bone volume fraction. Following Hosokawa and Otani [31], we use $n = 1.46$, $E = 2.2 \times 10^{10}$ and $\nu = 0.32$ for the exponent, Young modulus and Poisson ratio of solid (cortical) bone, respectively.

Table 10. Comparison between the NM and DE minima for $\eta = \eta_2$. Here, $N = 50$ for the high resolution and $N = 25$ for the low resolution.

ω	β	$f_{\min}$	% error
Guess/Target	0.7		
250 kHz			
NM	0.6983	0.1096	0.2429
DE	0.6983	0.1096	0.2429
Guess/Target	0.7		
500 kHz			
NM	0.7513	0.1542	7.329
DE	0.7513	0.1542	7.329
Guess/Target	0.83		
250 kHz			
NM	0.9044	0.9850	8.964
DE	0.9044	0.9850	8.964
Guess/Target	0.83		
500 kHz			
NM	0.8407	0.3091	1.289
DE	0.8407	0.3091	1.289
Guess/Target	0.9		
250 kHz			
NM	0.9029	0.2582	0.3222
DE	0.9029	0.2582	0.3222
Guess/Target	0.9		
500 kHz			
NM	0.8998	0.1911	0.0222
DE	0.9571	0.4379	6.344

- The imaginary parts of K_b and μ are calculated assuming a log decrement ℓ, i.e. $\operatorname{Im} K_b^* = \ell \operatorname{Re} K_b^*/\pi$ and $\operatorname{Im} \mu = \ell \operatorname{Re} \mu^*/\pi$ with $\ell = 0.1$, as typically used in underwater acoustics.[45]

These guesses have errors that are compounded mainly by two things: the error in our guess on β and the fact that these formulas are approximations to begin with. This leads us to question whether an alternative method to obtain guesses for Re K_b and Re μ may be more suitable. In the following section, we would like to obtain guesses for Re K_b and Re μ without considering them to be explicit functions of β.

5.2. *Multivariate minimization*

Having found guesses for the parameter β alone, we would like to determine if accurate guesses for Re K_b and Re μ can also be obtained. To produce these guesses, we use the DE algorithm. The reason for this choice is that it does not require a starting value. We use the same objective function (20) as previously. Bone porosity is fixed using the average of the guess values for β as given by the NM and DE schemes in Tables 9 and 10. By doing so,

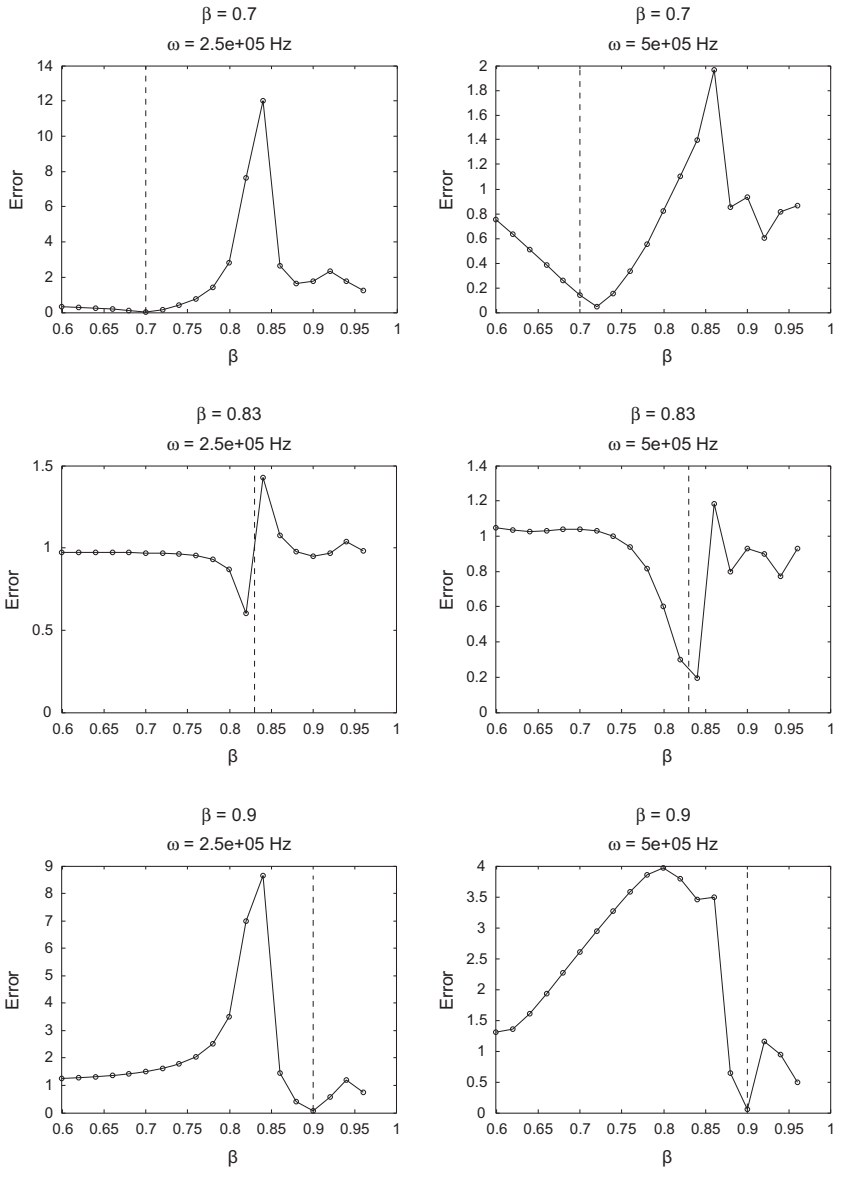

Figure 8. Sensitivity test on β for $\eta = \eta_2$. Here, $N = 90$ for the high resolution and $N = 65$ for the low resolution. The vertical dashed line corresponds to the target value of β specified in the high-resolution simulation. Both frequencies 250 and 500 kHz are considered.

we try to avoid some bias in the selection of β, although the average is not different from the guess values in most cases.

It can be seen from Tables 11 to 14 that we have varying degrees of success depending on the value of β, and we are able to recover the real part of μ with better accuracy. Importantly,

Table 11. Guesses for Biot parameters produced by the DE scheme in the case $\eta = \eta_1$.

ω	$f_{\min}$	β	Re K_b	Re μ
Guess/Target		0.7	3.5123e + 9	1.4369e + 9
250 kHz	0.2681	0.7032	4.5593e + 9	1.4151e + 9
500 kHz	0.1099	0.7251	9.5275e + 8	1.2933e + 9
Guess/Target		0.83	1.5327e + 9	6.2701e + 8
250 kHz	0.1988	0.8345	2.5792e + 9	5.9996e + 8
500 kHz	0.3866	0.8504	9.8725e + 8	5.1853e + 8
Guess/Target		0.9	7.0631e + 8	2.8895e + 8
250 kHz	0.5696	0.8898	5.7437e + 8	3.3229e + 8
500 kHz	0.1109	0.9033	7.6595e + 8	2.7407e + 8

Table 12. Guesses for Biot parameters produced by the DE scheme in the case $\eta = \eta_2$.

ω	$f_{\min}$	β	Re K_b	Re μ
Guess/Target		0.7	3.5123e + 9	1.4369e + 9
250 kHz	0.0903	0.6983	8.8536e + 8	1.4431e + 9
500 kHz	0.1309	0.7513	1.1369e + 9	1.0909e + 9
Guess/Target		0.83	1.5327e + 9	6.2701e + 8
250 kHz	0.9850	0.9044	1.6535e + 8	2.7056e + 8
500 kHz	0.3073	0.8407	1.0459e + 9	5.6728e + 8
Guess/Target		0.9	7.0631e + 8	2.8895e + 8
250 kHz	0.2537	0.9029	2.2512e + 8	2.7667e + 8
500 kHz	0.1655	0.9285	6.5012e + 8	2.7932e + 8

Table 13. Errors on the guesses obtained by the DE scheme for $\eta = \eta_1$.

ω	$f_{\min}$	β	Re K_b	Re μ
Guess/Target		0.7	3.5123e + 9	1.4369e + 9
250 kHz	0.2681	0.4571%	29.81%	1.52%
500 kHz	0.1099	3.600%	72.87%	9.99%
Guess/Target		0.83	1.5327e + 9	6.2701e + 8
250 kHz	0.1988	0.5422%	68.28%	4.31%
500 kHz	0.3866	2.4578%	35.39%	17.30%
Guess/Target		0.9	7.0631e + 8	2.8895e + 8
250 kHz	0.5696	1.1333%	18.68%	15.00%
500 kHz	0.1109	0.3667%	8.44%	5.15%

the orders of magnitude are well recovered in all cases. Based on this numerical evidence, it seems reasonable to use this model and scheme for producing guesses for the parameters of cancellous bone in the range of frequencies 250–500 kHz.

Table 14. Errors on the guesses obtained by the DE scheme for $\eta = \eta_2$.

ω	$f_{\min}$	β	Re K_b	Re μ
Guess/Target		0.7	3.5123e + 9	1.4369e + 9
250 kHz	0.0903	0.2429%	74.793%	0.4315%
500 kHz	0.1309	7.329%	67.631%	24.079%
Guess/Target		0.83	1.5327e + 9	6.2701e + 8
250 kHz	0.9844	8.964%	76.59%	6.364%
500 kHz	0.3073	1.289%	31.758%	9.526%
Guess/Target		0.9	7.0631e + 8	2.8895e + 8
250 kHz	0.2537	0.3222%	85.312%	55.874%
500 kHz	0.1654	6.344%	7.956%	3.331%

6. Conclusions

Upon comparison with Phase 1 tests in Buchanan and Gilbert [30], our numerical results in the present paper may be viewed as being successful. Except in one case, errors made on the guess for β were well under 10%. Recovery of Re K_b still proves troublesome; however, guesses here are more stable. Another success is the recovery of the parameter Re μ. Except in the extreme case where $\beta = 0.9$, we observe errors well below 34% on this guess, which is the lowest error obtained in Buchanan and Gilbert [30]. We would like to point out again that Buchanan and Gilbert [30] considered a simplified situation where the bone sample is an infinite slab, and they did not include effects of tortuosity in their model. The nicest feature of the present method of parameter recovery is that it does not require large sets of trial data, since the DE scheme requires no starting value.

If we compare with Table 1, our guesses for β and Re μ may be viewed again as successful. While errors may be slightly higher, we must note that our method of determining these guesses is significantly simpler, and does not require multiple initial guesses. Finally, we note that the change in viscosity does not significantly alter the error ranges on our results. With the experience gained from the present study, we plan to tackle the parameter recovery problem for the orthotropic case in the near future.

Funding

This research was partially supported by the NSF through [grant number DMS-0920850] and the Simons Foundation through [grant number 246170]. P. Guyenne thanks Prof. Masahiro Yamamoto and the Graduate School of Mathematical Sciences at the University of Tokyo for their hospitality during a visit in the summer 2013.

References

[1] Ashman RB, Cowin JD, Turner CH. Elastic properties of cancellous bone: measurement by ultrasonic technique. J. Biomech. 1987;10:979–989.

[2] Ashman RB, Rho JY. Elastic modulus of trabecular bone material. J. Biomech. 1988;21:177–181.

[3] Bossy E, Talmant M, Laugier P. Effect of bone cortical thickness on velocity measurements using ultrasonic axial transmission: a 2D simulation study. J. Acoust. Soc. Am. 2002;112:297–307.

[4] Chaffai S, Berger G, Laugier P. Frequency variation of ultrasonic attenuation coefficient of cancellous bone between 0.2 and 2.0 MHz. Proceedings of Ultrasonic Symposium; 1998; New York, NY. p. 1397–1400.
[5] Chaffai S, Roberjot V, Peyrin F, Berger G, Laugier P. Frequency dependence of ultrasonic backscattering in cancellous bone: autocorrelation model and experimental results. J. Acoust. Soc. Am. 2000;108:2403–2411.
[6] Droin P, Berger G, Laugier P. Velocity dispersion of acoustic waves in cancellous bone. IEEE Trans. Ultrason. Ferroelect. Freq. Control. 1998;45:581–592.
[7] Fellah ZEA, Chapelon Y, Berger S, Lauriks W, Depollier C. Ultrasonic wave propagation in human cancellous bone: application of Biot theory. J. Acoust. Soc. Am. 2004;116:61–73.
[8] Fellah M, Fellah Z, Mitri F, Ogam E, Depollier C. Transient ultrasound propagation in porous media using Biot theory and fractional calculus: application to human cancellous bone. J. Acoust. Soc. Am. 2013;133:1867–1881.
[9] Fry FJ, Barger JE. Acoustical properties of the human skull. J. Acoust. Soc. Am. 1978;63: 1576-1590.
[10] Haire TJ, Langton CM. Biot theory: a review of its application to ultrasound propagation through cancellous bone. Bone. 1999;24:291-295.
[11] Hobatho MC, Rho JY, Ashman RB. Atlas of mechanical properties of human cortical and cancellous bone. In: Van der Perre G, Lowet G, Borgwardt-Christensen A, editors. In Vivo assessment of bone quality by vibration and wave propagation techniques. Part 2. Durham (UK): ACCO; 1991. p. 7–38.
[12] Kaczmarek M, Pakula M, Kubik J. Multiphase nature and structure of biomaterials studied by ultrasound. Ultrasonics. 2000;38:703–707.
[13] Kundu T. Ultrasonic nondestructive evaluation. Boca Raton: CRC Press; 2004.
[14] Lakes RS, Yoon HS, Katz JL. Slow compressional wave propagation in wet human cortical bone. Science. 1992;220:513–515.
[15] Langton CM, Njeh CF. The physical measurement of bone. Bristol: Institute of Physics; 2004.
[16] Langton CM, Njeh CF, Hodgskinson R, Curey JD. Prediction of mechanical properties of human cancellous by broadbeam ultrasonic attenuation. Bone. 1996;18:495–503.
[17] Langton CM, Palmer SB, Porter RW. The measurement of broadband ultrasonic attenuation in cancellous bone. Eng. Med. 1984;13:89–91.
[18] McKelvie ML, Palmer SB. The interaction of ultrasound with cancellous bone. Phys. Med. Biol. 1991;10:1331–1340.
[19] Njeh CF, Hans D, Fuerst T, Gluer CC, Genant HK. Quantitative ultrasound assessment of osteoporosis and bone status. London: Martin Duniz; 1999. p. 391–399.
[20] Othman R, Gary G. Dispersion identification using the Fourier analysis of resonances in elastic and viscoelastic rods. In: Wirgin A, editor. Acoustics, mechanics, and the related topics of mathematical analysis. Singapore: World Scientific; 2002. p. 265–272.
[21] Padilla F, Peyrin F, Laugier P. Prediction of backscatter coefficient in trabecular bones using a numerical model of three-dimensional microstructure. J. Acoust. Soc. Am. 2003;113:1122–1129.
[22] Rho JY. An ultrasonic method for measuring the elastic properties of human tibial cortical and cancellous bone. Ultrasonics. 1996;34:777–783.
[23] Strelitzki R, Evans JA. On the measurement of the velocity of ultrasound in the calcis using short pulses. Eur. J. Ultrasound. 1996;4:205–213.
[24] Wear KA. Frequency dependence of ultrasonic backscatter from human trabecular bone: theory and experiment. J. Acoust. Soc. Am. 1999;106:3659–3664.
[25] Wear KA. Ultrasonic attenuation in human calcaneus from 0.2 to 1.7 MHz. IEEE Trans. Ultrason. Ferroelect. Freq. Control. 2001;48:602–608.
[26] Wear KA. Fundamental precision limitations for measurements of frequency dependence of backscatter: applications in tissue-mimicking phantoms and trabecular bone. J. Acoust. Soc. Am. 2001;110:3275–3282.

[27] Buchanan JL, Gilbert RP. Measuring osteoporosis using ultrasound. In: Fotiadis DI, Massalas CV, editors. Advances in scattering and biomedical engineering. Singapore: World Scientific; 2004. p. 484–494.
[28] Buchanan JL, Gilbert RP, Khashanah K. Determination of the parameters of cancellous bone using low frequency acoustic measurements. J. Comput. Acoust. 2004;12:99–126.
[29] Buchanan JL, Gilbert RP. Determination of the parameters of cancellous bone using high frequency acoustic measurements. Math. Comput. Model. 2007;45:281–308.
[30] Buchanan JL, Gilbert RP. Determination of the parameters of cancellous bone using high frequency acoustic measurements II: inverse problems. J. Comput. Acoust. 2007;15:199–220.
[31] Hosokawa A, Otani T. Ultrasonic wave propagation in bovine cancellous bone. J. Acoust. Soc. Am. 1997;101:558–562.
[32] Williams JL. Prediction of some experimental results by Biot's theory. J. Acoust. Soc. Am. 1992;91:1106–1112.
[33] Gluer CC. Quantitative ultrasound techniques for the assessment of osteoporosis: expert agreement on current status. J. Bone Miner. Res. 1997;12:1280–1288.
[34] Hoffmeister BK, Whitten SA, Rao JY. Low megahertz ultrasonic properties of bovine cancellous bone. Bone. 2000;26:635–642.
[35] Hodgskinson R, Njeh CF, Curey JD, Langton CM. The ability of ultrasound velocity to predict the stiffness of cancellous bone in vitro. Bone. 1997;21:183–190.
[36] Gilbert RP, Panchenko A, Vasilic A. Acoustic propagation in a random saturated medium: the monophasic case. Math. Meth. Appl. Sci. 2010;33:2206–2214.
[37] Gilbert RP, Panchenko A, Vasilic A. Homogenizing the acoustics of cancellous bone with an interstitial non-newtonian fluid. Nonlinear Anal. 2011;74:1005–1018.
[38] Gilbert RP, Panchenko A, Vasilic A. Acoustic propagation in a random saturated medium: the biphasic case. Appl. Anal. 2014;93:676–697.
[39] Gilbert RP, Guyenne P, Hsiao GC. Determination of cancellous bone density using low frequency acoustic measurements. Appl. Anal. 2008;87:1213–1225.
[40] Buchanan JL, Gilbert RP, Ou MY. Recovery of the parameters of cancellous bone by inversion of effective velocities, and transmission and reflection coefficients. Inverse Probl. 2011;27:1–23.
[41] Biot MA. Theory of propagation of elastic waves in a fluid-saturated porous solid. I. Lower frequency range. J. Acoust. Soc. Am. 1956;28:68–78.
[42] Biot MA. Mechanics of deformation and acoustic propagation in porous media. J. Appl. Phys. 1962;33:482–498.
[43] Stoll RD. Acoustic waves in saturated sediments. In: Hampton L, editor. Physics of sound in Marine sediments. New York (NY): Plenum; 1974.
[44] Biot MA. Theory of elasticity and consolidation for a porous anisotropic solid. J. Appl. Phys. 1955;26:182–185.
[45] Buchanan JL, Gilbert RP, Wirgin A, Xu YS. Marine acoustics: direct and inverse problems. Philadelphia (MA): SIAM; 2004.
[46] Johnson DL, Koplik J, Dashen R. Theory of dynamic permeability and tortuosity in fluid-saturated porous media. J. Fluid Mech. 1987;176:379–402.
[47] Isaacs A, Ray T, Smith W. A hybrid evolutionary algorithm with simplex local search. Proceedings of Congress on Evolutionary Computation; IEEE; 2007; New York, NY. p. 1701–1708.
[48] Price K, Storn R. Differential evolution – a simple and efficient heuristic for global optimization over continuous spaces. J. Global Optim. 1997;11:341–359.
[49] Nelder JA, Mead R. A simplex method for function minimization. Comput. J. 1965;7:308–313.
[50] Lagarias JC, Reeds JA, Wright MH, Wright PE. Convergence properties of the Nelder–Mead simplex method in low dimensions. SIAM J. Optim. 1998;9:112–147.
[51] Gilbert RP, Hsiao GC, Xu L. On the variational formulation of a transmision problem for the Biot equations. Appl. Anal. 2010;89:745–755.

[52] Hsiao GC, Kleinman RE, Roach GF. Weak solutions of fluid-solid interaction problems. Math. Nachr. 2000;218:139–163.
[53] Hsiao GC, Wendland LW. Boundary integral equations. Berlin: Springer-Verlag; 2008.

Appendix 1. Well posedness of the formulation

In the isotropic case,[51] it was shown using a variational approach that the Biot transmission problem is well posed. A variation of the same arguments may be used in the orthotropic case. We outline the procedure below on how this may be done by listing a sequence of theorems by which one may establish this result. The theorems are straightforward to establish by emulating the arguments of [51] (see also [52,53]). We begin by introducing several useful definitions.

Definition A.1 (Nonhomogeneous transmission problem (TP_f)) The problem consists of finding the triplet $(\mathbf{u}, s, P)$ such that

$$\left(\mu\mathbb{H}^{\top}+\frac{1}{1-\nu_1\nu_2}\mathbb{E}\mathbb{H}-\frac{p_{12}}{p_{22}}Q\mathbb{H}+p_{11}-\frac{p_{12}^2}{p_{22}}\right)\mathbf{u}-\left(\frac{p_{12}+Q\mathbb{H}}{p_{22}}\right)\nabla s=\mathbf{0}\quad\text{in}\quad\Omega^b,$$

and

$$\nabla^2 s+\frac{p_{22}}{R}s+\left(p_{12}-\frac{p_{22}Q}{R}\right)e=0\quad\text{in}\quad\Omega^b, \tag{A1}$$

$$-\left(\nabla^2 P+k_0^2 P\right)=f\quad\text{in}\quad\Omega^w, \tag{A2}$$

where $f:=-\nabla\cdot\mathbf{f}$, having compact support in Ω^w, together with the transmission conditions

$$\left[\underline{\underline{\sigma}}(\mathbf{u})+Q\nabla\cdot\mathbf{U}+s\right]\mathbf{n}=-P\,\mathbf{n}\quad\text{on}\quad\Gamma=\partial\Omega^b, \tag{A3}$$

$$\rho^w\omega^2\left[1-\beta\left(1+\frac{p_{12}}{p_{22}}\right)\right]\mathbf{u}\cdot\mathbf{n}-\frac{\beta\rho^w\omega^2}{p_{22}}\frac{\partial s}{\partial n}=\frac{\partial P}{\partial n}-\mathbf{n}\cdot\mathbf{f}\quad\text{on}\quad\Gamma, \tag{A4}$$

$$s=-\beta P\quad\text{on}\quad\Gamma, \tag{A5}$$

where $\underline{\underline{\sigma}}(\mathbf{u})$ and $\underline{\underline{\varepsilon}}(\mathbf{u})$ denote the stress and strain tensors,

$$\underline{\underline{\sigma}}(\mathbf{u})=\begin{pmatrix}\frac{E_1e_{11}+\nu_1E_2e_{22}}{1-\nu_1\nu_2} & \mu e_{12}\\ \mu e_{12} & \frac{E_2e_{22}+\nu_2E_1e_{11}}{1-\nu_1\nu_2}\end{pmatrix},$$

$$\underline{\underline{\varepsilon}}(\mathbf{u})=\frac{1}{2}\left(\nabla\mathbf{u}+\nabla\mathbf{u}^{\top}\right),$$

and the fluid dilatation is given by

$$\nabla\cdot\mathbf{U}=\frac{1}{R}\left(s-Q\,e\right).$$

In addition, we impose vanishing of the tangential frame stress $\sigma_{12}=\sigma_{21}=0$ on Γ and assume that the Sommerfeld radiation condition holds for P. In this formulation, transmission conditions (A3) and (A4) represent, respectively, the continuity of the flux and continuity of the aggregate pressure, while condition (A5) expresses the continuity of pore pressure.

For the uniqueness proof, we now introduce the traction-free solution for the bone as in fluid–structure interaction problems.[52]

Definition A.2 (Traction-free problem) The problem for $(\mathbf{u}, s)$ in Ω^b consists of the partial differential Equations (A1) and (A2) together with the homogeneous boundary conditions

$$\left[\underline{\underline{\sigma}}(\mathbf{u}) + Q\nabla\cdot\mathbf{U} + s\right]\mathbf{n} = \mathbf{0} \quad \text{on} \quad \Gamma,$$
$$\rho^w\omega^2\left[1-\beta\left(1+\frac{p_{12}}{p_{22}}\right)\right]\mathbf{u}\cdot\mathbf{n} - \frac{\beta\rho^w\omega^2}{p_{22}}\frac{\partial s}{\partial n} = \frac{\partial P}{\partial n} \quad \text{on} \quad \Gamma,$$
$$s = 0 \quad \text{on} \quad \Gamma,$$

which is called the traction-free problem for $(\mathbf{u}, s)$, and the corresponding nontrivial solutions are referred to as the traction-free solutions.

For the variational formulation, we now reduce the partial differential Equation (A2) for P to a boundary integral equation on Γ. We use the indirect approach for the reduction of partial differential equations by seeking a solution P in the form of a single-layer potential

$$P = -\mathbf{S}\phi + P_f \quad \text{in} \quad \Omega^w, \tag{A6}$$

where ϕ is an unknown density function and $\mathbf{S}\phi$ is the single-layer potential

$$\mathbf{S}\phi(\mathbf{x}) := \frac{i}{4}\int_\Gamma H_0^{(1)}(k_0\|\mathbf{x}-\mathbf{y}\|)\phi(\mathbf{y})\,\mathrm{d}s_y, \quad \mathbf{x}\in\Omega^w,$$

where $-i\,H_0^{(1)}/4$ denotes the fundamental solution of the Helmholtz operator $\nabla^2 + k_0^2$, and

$$P_f(\mathbf{x}) := \frac{i}{4}\int_{\mathrm{supp}(f)} H_0^{(1)}(k_0\|\mathbf{x}-\mathbf{y}\|)\,f(\mathbf{y})\,d\mathbf{y}, \quad \mathbf{x}\in\Omega^w,$$

is a particular solution of (A2), which is known. Hence, if $P|_\Gamma$ is given, by applying the trace operator γ_0 to (A6), we obtain a boundary integral equation for the known density ϕ,

$$P|_\Gamma = -\mathbf{V}\phi + \gamma_0 P_f, \tag{A7}$$

where $\mathbf{V} = \gamma_0\mathbf{S}$ is the single-layer boundary integral operator. Then from the transmission condition (B_3), we arrive at the boundary integral equation

$$\mathbf{V}\phi - \frac{1}{\beta}s = \gamma_0 P_f. \tag{A8}$$

Definition A.3 (Nonlocal boundary value problem) The TP_f is termed a nonlocal boundary value problem for the triplet $(\mathbf{u}, s, \phi)$ if the latter satisfies (A1), (A2) and the boundary integral Equation (A8), together with the transmission conditions (A3), (A7) and (A4) where

$$\frac{\partial P}{\partial n} = \frac{1}{2}\phi - \mathbf{K}\phi + \frac{\partial P_f}{\partial n}.$$

The boundary integral operator $\mathbf{K}$ is defined by

$$\mathbf{K}\phi(\mathbf{x}) := \frac{i}{4}\int_\Gamma \frac{\partial H_0^{(1)}}{\partial n}(k_0\|\mathbf{x}-\mathbf{y}\|)\phi(\mathbf{y})\,\mathrm{d}s_y, \quad \mathbf{x}\in\Gamma,$$

where the normal derivative is taken with respect to $\mathbf{x}$. We note that condition (A4) can be explicitly written in terms of ϕ as

$$\frac{\partial s}{\partial n} = \frac{p_{22}}{\beta}\left\{\left[1-\beta\left(1+\frac{p_{12}}{p_{22}}\right)\right]\mathbf{u}\cdot\mathbf{n} - \frac{1}{\rho^w\omega^2}\left(\frac{1}{2}\phi - \mathbf{K}\phi\right)\right\} + \frac{p_{22}}{\beta\rho^w\omega^2}\left(\mathbf{n}\cdot\mathbf{f} - \frac{\partial P_f}{\partial n}\right),$$

which will be needed for the variational formulation in the next section.

Appendix 2. Variational formulation

We consider the variational formulation of the nonlocal boundary value problem using the ideas of [51]. As usual, by multiplying (A8) with the conjugate of a test vector $\mathbf{v}$ and integrating by parts, we obtain

$$\begin{aligned}\int_{\Omega^b}\Bigg[&\frac{1}{1-\nu_1\nu_2}\begin{pmatrix} E_1e_{11}+\nu_1E_2e_{22} & 0\\ 0 & \nu_2E_1e_{11}+E_2e_{22}\end{pmatrix} : \overline{\underline{\underline{e}}(\mathbf{v})} + 2\mu\,\underline{\underline{\varepsilon}}(\mathbf{u}) : \overline{\underline{\underline{\varepsilon}}(\mathbf{v})}\\ &- \frac{Q^2}{R}(\nabla\cdot\mathbf{u})\,(\nabla\cdot\overline{\mathbf{v}}) + \left(\frac{Q}{R}-\frac{p_{12}}{p_{22}}\right)s\,\nabla\cdot\overline{\mathbf{v}} - \left(p_{11}-\frac{p_{12}^2}{p_{22}}\right)\mathbf{u}\cdot\overline{\mathbf{v}}\Bigg]\,d\mathbf{x}\\ &-\int_\Gamma\Bigg[\begin{pmatrix} E_1e_{11}+\nu_1E_2e_{22} & 0\\ 0 & \nu_2E_1e_{11}+E_2e_{22}\end{pmatrix} :\, 2\mu\,\underline{\underline{\varepsilon}}(\mathbf{u}) - \frac{Q^2}{R}\nabla\cdot\mathbf{u} + \left(\frac{Q}{R}-\frac{p_{12}}{p_{22}}\right)s\Bigg]\\ &\times\mathbf{n}\cdot\overline{\mathbf{v}}\,\mathrm{d}s = 0.\end{aligned} \tag{B1}$$

We define the sesquilinear bilinear form

$$a(\mathbf{u},\mathbf{v}) := \int_{\Omega^b}\left[\frac{1}{1-\nu_1\nu_2}\begin{pmatrix} E_1e_{11}+\nu_1E_2e_{22} & 0\\ 0 & \nu_2E_1e_{11}+E_2e_{22}\end{pmatrix} : \overline{\underline{\underline{e}}(\mathbf{v})} + 2\mu\,\underline{\underline{\varepsilon}}(\mathbf{u}) : \overline{\underline{\underline{\varepsilon}}(\mathbf{v})}\right]d\mathbf{x},$$

and by rewriting the boundary term in (B1), we see that

$$\begin{aligned}&a(\mathbf{u},\mathbf{v}) + \int_{\Omega^b}\left(\frac{Q}{R}-\frac{p_{12}}{p_{22}}\right)s\,\nabla\cdot\overline{\mathbf{v}}\,d\mathbf{x} - \int_{\Omega^b}\left(p_{11}-\frac{p_{12}^2}{p_{22}}\right)\mathbf{u}\cdot\overline{\mathbf{v}}\,d\mathbf{x}\\ &+\int_\Gamma\left(1+\frac{p_{12}}{p_{22}}\right)s\,\mathbf{n}\cdot\overline{\mathbf{v}}\,\mathrm{d}s - \int_\Gamma\left[\lambda\,\nabla\cdot\mathbf{u} + 2\mu\,\underline{\underline{\varepsilon}}(\mathbf{u}) + \frac{Q}{R}(s - Q\,\nabla\cdot\mathbf{u}) + s\right]\mathbf{n}\cdot\overline{\mathbf{v}}\,\mathrm{d}s \;=\; 0.\end{aligned}$$

Hence, the above equation with the transmission condition (A8) leads to the variational equation

$$\begin{aligned}&a(\mathbf{u},\mathbf{v}) + \int_{\Omega^b}\left(\frac{Q}{R}-\frac{p_{12}}{p_{22}}\right)s\,\nabla\cdot\overline{\mathbf{v}}\,d\mathbf{x} - \int_{\Omega^b}\left(p_{11}-\frac{p_{12}^2}{p_{22}}\right)\mathbf{u}\cdot\overline{\mathbf{v}}\,d\mathbf{x}\\ &-\left[1-\beta\left(1+\frac{p_{12}}{p_{22}}\right)\right]\langle\mathbf{V}\phi\,\mathbf{n},\overline{\mathbf{v}}\rangle_\Gamma = -\left[1-\beta\left(1+\frac{p_{12}}{p_{22}}\right)\right]\langle\gamma_0P_f,\overline{\mathbf{v}}\rangle_\Gamma, \qquad \forall\,\mathbf{v}\in\left(H^1(\Omega^b)\right)^2.\end{aligned} \tag{B2}$$

Repeating this process for the s-equation by multiplying (A1) with the conjugate of a test function τ and integrating by parts leads to the variational equation

$$\begin{aligned}&b(s,\tau) + p_{22}\int_{\Omega^b}\left(\frac{Q}{R}-\frac{p_{12}}{p_{22}}\right)(\nabla\cdot\mathbf{u})\,\overline{\tau}\,d\mathbf{x} - \int_{\Omega^b}\frac{p_{22}}{R}s\,\overline{\tau}\,d\mathbf{x}\\ &\quad-\frac{p_{22}}{\beta}\left[1-\beta\left(1+\frac{p_{12}}{p_{22}}\right)\right]\langle\mathbf{u}\cdot\mathbf{n},\overline{\tau}\rangle_\Gamma + \frac{p_{22}}{\beta\rho^w\omega^2}\left\langle\frac{1}{2}\phi-\mathbf{K}\phi,\overline{\tau}\right\rangle_\Gamma\\ &\quad=\frac{p_{22}}{\beta\rho^w\omega^2}\left\langle\mathbf{n}\cdot\mathbf{f}-\frac{\partial P_f}{\partial n},\overline{\tau}\right\rangle_\Gamma, \quad \forall\,\tau\in H^1(\Omega^b),\end{aligned} \tag{B3}$$

where $b(s,\tau)$ is the sesquilinear form

$$b(s,\tau) = \int_{\Omega^b}\nabla s\cdot\nabla\overline{\tau}\,d\mathbf{x}.$$

Following [51], the boundary integral Equation (A8) may be put into variational form as

$$\frac{p_{22}}{2\rho^w\omega^2}\langle\mathbf{V}\phi,\overline{\psi}\rangle_\Gamma - \frac{p_{22}}{2\rho^w\omega^2\beta}\langle s,\overline{\psi}\rangle_\Gamma = \frac{p_{22}}{2\rho^w\omega^2}\langle\gamma_0P_f,\overline{\psi}\rangle_\Gamma, \quad \forall\,\psi\in H^{-1/2}(\Gamma). \tag{B4}$$

Collecting (B2)–(B4), we have the variational formulation for the nonlocal boundary value problem.

Definition B.1 (Variational formulation) Given $\mathbf{f}$, find the triplet $(\mathbf{u}, s, \phi) \in \left(H^1(\Omega^b)\right)^2 \times H^1(\Omega^b) \times H^{-1/2}(\Gamma)$ such that

$$\mathcal{A}\Big\{(\mathbf{u}, s, \phi), (\mathbf{v}, \tau, \psi)\Big\} = \mathcal{L}_f(\mathbf{v}, \tau, \psi), \tag{B5}$$

for all $(\mathbf{v}, \tau, \psi) \in \left(H^1(\Omega^b)\right)^2 \times H^1(\Omega^b) \times H^{-1/2}(\Gamma)$, where $\mathcal{A}$ and $\mathcal{L}_f$ are, respectively, the sesquilinear form and linear functional defined by

$$\begin{aligned}
\mathcal{A}\Big\{(\mathbf{u}, s, \phi), (\mathbf{v}, \tau, \psi)\Big\} &:= a(\mathbf{u}, \mathbf{v}) + b(s, \tau) + \frac{p_{22}}{2\rho^w\omega^2}\left\langle \mathbf{V}\phi, \overline{\psi}\right\rangle_\Gamma \\
&\quad + \left(\frac{Q}{R} - \frac{p_{12}}{p_{22}}\right)\left(\int_{\Omega^b} s\,\nabla\cdot\overline{\mathbf{v}}\,d\mathbf{x} + p_{22}\int_{\Omega^b}(\nabla\cdot\mathbf{u})\,\overline{\tau}\,d\mathbf{x}\right) \\
&\quad - \left(p_{11} - \frac{p_{12}^2}{p_{22}}\right)\int_{\Omega^b}\mathbf{u}\cdot\overline{\mathbf{v}}\,d\mathbf{x} - \frac{p_{22}}{R}\int_{\Omega^b} s\,\overline{\tau}\,d\mathbf{x} \\
&\quad - \left[1 - \beta\left(1 + \frac{p_{12}}{p_{22}}\right)\right]\left(\langle \mathbf{V}\phi\,\mathbf{n}, \overline{\mathbf{v}}\rangle_\Gamma + \frac{p_{22}}{\beta}\langle \mathbf{u}\cdot\mathbf{n}, \overline{\tau}\rangle_\Gamma\right) \\
&\quad + \frac{p_{22}}{\beta\rho^w\omega^2}\left(\left\langle\frac{1}{2}\phi - \mathbf{K}\phi, \overline{\tau}\right\rangle_\Gamma - \frac{1}{2}\langle s, \overline{\psi}\rangle_\Gamma\right), \\
\mathcal{L}_f(\mathbf{v}, \tau, \psi) &:= -\left[1 - \beta\left(1 + \frac{p_{12}}{p_{22}}\right)\right]\langle\gamma_0 P_f, \overline{\mathbf{v}}\rangle_\Gamma + \frac{p_{22}}{\beta\rho^w\omega^2}\left\langle \mathbf{n}\cdot\mathbf{f} - \frac{\partial P_f}{\partial n}, \overline{\tau}\right\rangle_\Gamma \\
&\quad + \frac{p_{22}}{2\rho^w\omega^2}\langle\gamma_0 P_f, \overline{\psi}\rangle_\Gamma\,.
\end{aligned} \tag{B6}$$

Appendix 3. Existence and uniqueness

From the definition of the sesquilinear form $\mathcal{A}(\cdot,\cdot)$ in (B6), it is not difficult to see that $\mathcal{A}(\cdot,\cdot)$ satisfies a Gårding's inequality. Setting $(\mathbf{v}, \tau, \psi) = (\mathbf{u}, s, \phi)$, we obtain

$$\begin{aligned}
\mathcal{A}\Big\{(\mathbf{u}, s, \phi), (\mathbf{u}, s, \phi)\Big\} &:= a(\mathbf{u}, \mathbf{u}) + b(s, s) + \frac{p_{22}}{2\rho^w\omega^2}\left\langle \mathbf{V}\phi, \overline{\phi}\right\rangle_\Gamma \\
&\quad + \left(\frac{Q}{R} - \frac{p_{12}}{p_{22}}\right)\left(\int_{\Omega^b} s\,\nabla\cdot\overline{\mathbf{u}}\,d\mathbf{x} + p_{22}\int_{\Omega^b}(\nabla\cdot\mathbf{u})\,\overline{s}\,d\mathbf{x}\right) \\
&\quad - \left(p_{11} - \frac{p_{12}^2}{p_{22}}\right)\int_{\Omega^b}\|\mathbf{u}\|^2 d\mathbf{x} - \frac{p_{22}}{R}\int_{\Omega^b}|s|^2 d\mathbf{x} \\
&\quad - \left[1 - \beta\left(1 + \frac{p_{12}}{p_{22}}\right)\right]\left(\langle \mathbf{V}\phi\,\mathbf{n}, \overline{\mathbf{u}}\rangle_\Gamma + \frac{p_{22}}{\beta}\langle \mathbf{u}\cdot\mathbf{n}, \overline{s}\rangle_\Gamma\right) \\
&\quad + \frac{p_{22}}{\beta\rho^w\omega^2}\left(\left\langle\frac{1}{2}\phi - \mathbf{K}\phi, \overline{s}\right\rangle_\Gamma - \frac{1}{2}\langle s, \overline{\phi}\rangle_\Gamma\right).
\end{aligned} \tag{C1}$$

We can show that

$$\mathrm{Re}\,\mathcal{A}\Big\{(\mathbf{u}, s, \phi), (\mathbf{u}, s, \phi)\Big\} = a(\mathbf{u}, \mathbf{u}) + b(s, s) + \frac{p_{22}}{2\rho^w\omega^2}\left\langle \mathbf{V}\phi, \overline{\phi}\right\rangle_\Gamma + \mathcal{C}\Big\{(\mathbf{u}, s, \phi), (\mathbf{u}, s, \phi)\Big\},$$

where $\mathcal{C}$ is compact on $\left(H^1(\Omega^b)\right)^2 \times H^1(\Omega^b) \times H^{-1/2}(\Gamma)$. In fact, we have:

THEOREM C.1 *The sesquilinear form in (C1) satisfies the Gårding's inequality in the form*

$$\begin{aligned}
\mathrm{Re}\,\mathcal{A}\Big\{(\mathbf{u}, s, \phi), (\mathbf{u}, s, \phi)\Big\} &\geq \alpha\left(\|\mathbf{u}\|^2_{\left(H^1(\Omega^b)\right)^2} + \|s\|^2_{H^1(\Omega^b)} + \|\phi\|^2_{H^{-1/2}(\Gamma)}\right) \\
&\quad -\delta\left(\|\mathbf{u}\|^2_{\left(H^{1-\epsilon}(\Omega^b)\right)^2} + \|s\|^2_{H^{1-\epsilon}(\Omega^b)} + \|\phi\|^2_{H^{-1/2-\epsilon}(\Gamma)}\right),
\end{aligned}$$

where $\alpha > 0$ and $\delta \geq 0$ are constants, and $\epsilon > 0$ is a small parameter.

As is well known, Gårding's inequality implies the validity of the Fredholm alternative. Hence, uniqueness implies existence. For this purpose, we now consider the homogeneous TP_f with $f = 0$, since the uniqueness of the solution to the variational Equation (B5) will be depending upon that of the TP_f.

THEOREM C.2 *If the triplet $(\mathbf{u}, s, P)$ is a classical solution of the homogeneous TP_0 with $Im\, k_0 = 0$, then $P = 0$.*

The proof follows [51] and the reader can supply the details. We remark that this theorem does imply that the components $(\mathbf{u}, s)$ of the triplet $(\mathbf{u}, s, P)$ considered in the TP_0 are trivial solutions, since they may be solutions of the traction-free problem. Hence, in order to ensure the existence of a solution to the variational Equation (B5), we make the following assumptions:

(1) There is no traction-free solution.
(2) The square of the wavenumber, k_0^2, is not an eigenvalue of the Dirichlet problem for the negative Laplacian in Ω^b.

We remark that Assumption (2) is a guarantee for the invertibility of the single-layer operator $\mathbf{V}$ (see [53, p.30]). We finally summarize our results in the following theorem.

THEOREM C.3 *Under Assumptions* (1) *and* (2)*, there exists a unique solution of the* TP_f *in* $\left(H^1(\Omega^b)\right)^2 \times H^1(\Omega^b) \times H^{-1/2}(\Gamma)$.